

<https://doi.org/10.1038/s42003-024-06601-y>

# OLFM4 modulates intestinal inflammation by promoting IL-22<sup>+</sup> ILC3 in the gut



Zhe Xing<sup>1,8</sup>, Xinyao Li<sup>2,8</sup>, Junyu He<sup>2,8</sup>, Yimin Chen<sup>2,8</sup>, Lei Zhu<sup>3</sup>, Xiaogang Zhang<sup>2</sup>, Zhengcong Huang<sup>2</sup>, Jian Tang<sup>4,5,6,9</sup> ✉, Yuxiong Guo<sup>7,9</sup> ✉ & Yumei He<sup>1,2,9</sup> ✉

Group 3 innate lymphoid cells (ILC3s) play key roles in intestinal inflammation. Olfactomedin 4 (OLFM4) is highly expressed in the colon and has a potential role in dextran sodium sulfate-induced colitis. However, the detailed mechanisms underlying the effects of OLFM4 on ILC3-mediated colitis remain unclear. In this study, we identify OLFM4 as a positive regulator of IL-22<sup>+</sup> ILC3. OLFM4 expression in colonic ILC3s increases substantially during intestinal inflammation in humans and mice. Compared to littermate controls, OLFM4-deficient (OLFM4<sup>-/-</sup>) mice are more susceptible to bacterial infection and display greater resistance to anti-CD40 induced innate colitis, together with impaired IL-22 production by ILC3, and ILC3s from OLFM4<sup>-/-</sup> mice are defective in pathogen resistance. Besides, mice with OLFM4 deficiency in the ROR $\gamma$ t compartment exhibit the same trend as in OLFM4<sup>-/-</sup> mice, including colonic inflammation and IL-22 production. Mechanistically, the decrease in IL-22<sup>+</sup> ILC3 caused by OLFM4 deficiency involves the apoptosis signal-regulating kinase 1 (ASK1)- p38 MAPK signaling-dependent downregulation of RAR-related orphan receptor gamma (ROR $\gamma$ t) protein. The OLFM4-metadherin (MTDH) complex upregulates p38/ROR $\gamma$ t signaling, which is necessary for IL-22<sup>+</sup> ILC3 activation. The findings indicate that OLFM4 is a novel regulator of IL-22<sup>+</sup> ILC3 and essential for modulating intestinal inflammation and tissue homeostasis.

Innate lymphoid cells (ILCs) are tissue-resident cells that lack rearranged antigen-specific receptors. These cells develop from common lymphoid progenitor cells and are morphologically and functionally similar to adaptive lymphocytes<sup>1</sup>. ILCs are divided into three subgroups based on their expression of transcription factors and cytokines: ILC1, ILC2, and ILC3<sup>2-6</sup>. ILC3s are highly enriched in the gut, where they mediate innate immune response and immune tolerance, and produce interleukin (IL)-17 and/or IL-22 as well as granulocyte-macrophage colony-stimulating factor (GM-CSF) under the control of the RAR-related orphan receptor gamma (ROR $\gamma$ t) and aryl hydrocarbon receptors<sup>7,8</sup>. Emerging evidence indicates that ILC3s are important regulators of intestinal barrier integrity, microbiota homeostasis, resolution of local inflammation, and restoration of homeostasis via cytokine release<sup>9-11</sup>. ILC3s are responsive to cytokines IL-23 and IL-1 $\beta$ , which are produced by intestinal mononuclear phagocyte populations and drive ILC3 function<sup>12-14</sup>. Additionally, the gut environment has a critical impact on ILC3s and cell responses. Dietary metabolites, such as short-chain fatty acids, oxysterols, and butyrate, can directly activate ILC3s through the metabolite receptor free fatty acid receptor 2 (FFAR2)<sup>15-17</sup>. In addition to dietary ligands, retinoic acid and vitamin D can also regulate ILC3 activity<sup>18,19</sup>, and intestinal cells directly regulate ILC3s via cytokines or the nervous system. For example, IL-17D expressed by intestinal epithelial cells

(IECs) can activate ILC3s via the CD93 receptor<sup>20</sup>. Vasoactive intestinal protein (VIP) derived from the enteric nervous system can markedly enhanced the production of IL-22 in ILC3 through activation of vasoactive intestinal peptide receptor 2 (VIPR2)<sup>21-23</sup>. Despite considerable recent progress, the functional mechanisms of several proteins with crucial regulatory roles in ILC3s remain poorly understood.

Patients with ulcerative colitis (UC) have lower frequencies of IL-22-producing ILC3s and impaired IL-22 function in their intestines compared to healthy controls, leading to intestinal dysfunction<sup>24</sup>. Similar to inflammatory bowel disease (IBD) and enterohemorrhagic and enteropathogenic *Escherichia coli* infections in humans, the early stage of antibacterial immunity was regulated by ILC3s in a *Citrobacter rodentium* (*C. rodentium*) -infection mouse model<sup>25</sup>. The production of inflammatory cytokines, such as IL-1 $\beta$  and IL-23, enables ILC3s to rapidly respond to IL-22 and IL-17 production, promoting neutrophil recruitment to the intestinal tract and enabling IECs to produce antimicrobial peptides (AMPs) and mucus. An IL-22 fate reporter showed that the main source of IL-22 in the first 5 days after infection was ILC3, whereas thereafter CD4<sup>+</sup> T cells were the main source<sup>26</sup>. In contrast, overactivated ILC3s produce abundant IL-22, IL-17A, GM-CSF, and IFN- $\gamma$ , which also leads to colitis<sup>27</sup>. The anti-CD40-induced colitis mouse model is a classic example by which dysregulated ILC3s

A full list of affiliations appears at the end of the paper. ✉ e-mail: [tangj33@mail.sysu.edu.cn](mailto:tangj33@mail.sysu.edu.cn); [guoyuxiong@gdph.org.cn](mailto:guoyuxiong@gdph.org.cn); [hym0909@smu.edu.cn](mailto:hym0909@smu.edu.cn)

initiate and enhance the progression of chronic intestinal inflammation through cytokines<sup>12,28</sup>.

Previous studies suggested that intestinal epithelial regeneration is crucial for maintaining intestinal homeostasis and repairing the mucosal barrier<sup>29</sup>. Leucine-rich repeat-containing G protein-coupled receptor 5-positive (LGR5<sup>+</sup>) crypt basal columnar cells (CBCs), located at the base of the crypt region, are the source of intestinal epithelial renewal<sup>30</sup>. Olfactomedin-4 (OLFM4) glycoprotein has been used as a specific marker for LGR5<sup>+</sup> CBCs in the human small intestine and colon<sup>31</sup>. Moreover, OLFM4 expression is upregulated during inflammation. It has been reported that higher levels of OLFM4 expression have been observed in the inflamed mucosa of patients with IBD<sup>32,33</sup> and the gastric mucosa of patients infected with *Helicobacter pylori*<sup>34</sup>. Another study reported that OLFM4-deficient mice with DSS-induced colitis presented with more severe inflammation and mucosal damage than wild-type (WT) mice<sup>35</sup>. The above studies have focused on OLFM4, which may play a key role in the regulation of inflammation. Ample evidence suggests that ILC3s are crucial in protecting the gut from microbiota disorders through IL-22-mediated regulation of AMPs, such as *RegIIIβ* and *RegIIIγ*, and in repairing damage by promoting the proliferation of LGR5<sup>+</sup> intestinal epithelial stem cells<sup>36–38</sup>. Implying OLFM4 may be critical for protecting the host against acute intestinal inflammation. Therefore, we investigated the role of OLFM4 in ILC3-driven intestinal inflammation.

We first reanalyzed the previously reported single-cell sequencing results of patients with UC<sup>39</sup>. In intestinal tissue-derived ILC3 cells, OLFM4 expression was upregulated compared to that in control. Subsequent data from mice with OLFM4<sup>-/-</sup> and OLFM4 deficiency in the RORc compartments (RORc<sup>Cre</sup>OLFM4<sup>fl/fl</sup> mice) revealed increased susceptibility to bacterial infection and greater resistance to anti-CD40-induced innate colitis, along with impaired IL-22 production by ILC3. Furthermore, adoptive transfer of ILC3s into NCG mice (Rag2<sup>-/-</sup> Il2ry<sup>-/-</sup>, lacking of T, B, ILCs and NK cells) demonstrated that OLFM4 deficiency significantly impairs ILC3 function. And bone marrow transplantation (BMT) revealed that the regulation of OLFM4 on intestinal inflammation is mainly driven by ILC3. We subsequently verified that OLFM4 regulates ILC3 function through the apoptosis signal-regulating kinase 1 (ASK1)-p38/RORγt/IL-22 axis and determined that the OLFM4-metadherin (MTDH) complex is required for the activation of this signaling pathway. These findings revealed the critical role of OLFM4 in regulating IL-22<sup>+</sup> ILC3 in innate colitis.

## Results

### OLFM4 is highly expressed in murine and human intestinal ILC3s

OLFM4 is highly expressed in human and mouse intestines and bone marrow<sup>40,41</sup>. To explore the role of OLFM4 in intestinal diseases, we firstly assessed the expression level of OLFM4 in patients with ulcerative colitis (UC), and an inducible expression of OLFM4 was observed in intestinal biopsies from UC patients based on RNA-sequence data from the Gene Expression Omnibus (GEO) profiling database (GSE48634) (Fig. S1A, B). An increase protein level of OLFM4 in the intestine from DSS-induced colitis mice was next identified by western blotting (Fig. S1C, D). Additional, reanalyzing the single-cell sequencing results of patients with UC described by Smillie et al. (2019, accession number SCP259)<sup>39</sup> revealed that OLFM4 expression was upregulated in intestinal tissue-derived ILC3s (ILC3s were identified by lineage (CD3, CD4, CD56, CD11b, CD11c)<sup>-</sup>CD127<sup>+</sup>CRTH2<sup>+</sup> followed by co-expression of Nkp44 and c-kit) from patients with UC (Fig. S2A). Consistent with the single-cell sequencing results, OLFM4 were found to be upregulated in ILC3s derived from intestinal tissue of UC patients compared with that from controls (Fig. 1A), and immunofluorescence staining also confirmed that OLFM4 was highly expressed in intestinal ILC3s (CD3<sup>-</sup>RORγt<sup>+</sup>OLFM4<sup>+</sup>) in patients with UC (Figs. 1B and S2B, C). Next, we investigated the expression of OLFM4 in ILC3 of human peripheral blood mononuclear cells (PBMC) from patients with UC and that from healthy volunteers (HC). Data showed that the clinicopathological severity of UC is accompanied by increased expression of OLFM4 in ILC3 from PBMC (Fig. 1C). Correlation analysis of the

relationship between OLFM4 expression and the clinicopathological severity of UC, the Mayo Score, demonstrated that disease severity was positively associated with OLFM4 expression (Fig. 1D). These data suggest that OLFM4 is upregulated in ILC3s in human UC. We hence conducted some experiments in mice to validate human data. OLFM4 expression in different tissues revealed that OLFM4 highly expressed in gut-associated tissues, such as colon, small intestine, mesenteric lymph nodes (mLN) and Peyer's patches (PP), compared with the spleen (SP), bone marrow (BM) and peripheral blood mononuclear cells (PBMC) (Fig. S3A). Several studies have shown that OLFM4 exhibits high expression levels in neutrophils, PMN-MDSCs, and intestinal cells within murine colitis models<sup>33,42,43</sup>. OLFM4 expression in different immune cells in the inflamed colon were firstly investigated. Huge expression of OLFM4 in neutrophils was observed as expected (Fig. S3B), OLFM4 was also abundantly expressed in ILC3s, but low expression on T cells, macrophages and almost no expression on B cells (Fig. S3B). Given OLFM4 is highly expressed in inflamed intestinal cells<sup>42</sup>, we subsequently explored its expression level in epithelial cells, endothelial cells and ILC3 in inflamed colon. Results showed that OLFM4 expression in ILC3 is significantly higher than that in CD45<sup>-</sup>CD31<sup>+</sup> epithelial cells and CD45<sup>-</sup>CD31<sup>+</sup> endothelial cells from colonic lamina propria cells of colitis mice (Fig. S3C). Similar observations were noted in ILC1 and ILC2, enriched in inflamed colon, indicated by higher expression of OLFM4 in ILC3 than ILC1 and ILC2 both at protein and mRNA levels (Fig. S3D, E). These observations implied that OLFM4 may play a role in intestinal inflammation regulated by ILC3. We therefore examined the expression pattern of OLFM4 in ILC3s in both *C. rodentium* infection and DSS induced colitis models. Similar to the results observed in humans, OLFM4 expression was markedly increased in colonic ILC3s (CD3<sup>-</sup>RORγt<sup>+</sup>OLFM4<sup>+</sup>) from *C. rodentium* infection and DSS induced colitis mice (Figs. 1E and S4A). Flow cytometric analysis also showed that OLFM4 expression in ILC3s from LPMC was significantly increased in inflamed colon (Figs. 1F and S4B, C), and the expression of OLFM4 in ILC3s exhibits a positive correlation with pathological severity of colitis (Fig. 1G, H). The mRNA expression level of OLFM4 in colon ILC3s further confirmed above data (Fig. 1I). Besides, we examined the expression of OLFM4 in ILC3 subsets obtained from murine colonic tissue<sup>44</sup>. Results showed that OLFM4 is expressed at a significantly higher level in Nkp46<sup>+</sup> ILC3 cells under physiological conditions and both colitis models compared to CCR6<sup>+</sup> ILC3s and double negative ILC3s (Figs. 1J and S5A–C). Considering the role of the CD4<sup>+</sup>RORγt<sup>+</sup> cells in regulating intestinal inflammation<sup>45</sup>, we next evaluated OLFM4 expression in CD4<sup>+</sup>RORγt<sup>+</sup> cells in both *C. rodentium* infection and DSS-induced colitis mice. Data showed that no noticeable differences were observed from OLFM4 expression in CD4<sup>+</sup>RORγt<sup>+</sup> cells between control and colitis mice (Fig. S6). These data suggested that potential role of OLFM4 in ILC3-driven intestinal inflammation.

### OLFM4 deficiency impaired ILC3 function and pathogen resistance

To better understand the potential role of OLFM4 in regulating intestinal homeostasis and disease progression through ILC3, we firstly investigated the effect of OLFM4 deletion on intestinal tract and ILC3 level under steady-state conditions. Data showed that no significant alterations was presented both in intestinal length and spleen weight (Fig. S7A–D), as well as the proportion and number of ILC3s in LPMCs between OLFM4<sup>-/-</sup> and WT mice (Fig. S8A, B). A slight lower of IL-22<sup>+</sup> ILC3 and IL-17<sup>+</sup> ILC3 level and absolute number from OLFM4<sup>-/-</sup> mice, compared with WT mice (Fig. S8C–F). Given OLFM4<sup>-/-</sup> mice develop more severe inflammation and mucosal damage under DSS-induced colitis<sup>35,46</sup>, we postulated the involvement of OLFM4 in the regulation of ILC3-mediated acute colitis, as evidenced by its upregulated expression in inflamed colonic ILC3s. To test this hypothesis, we next established a *C. rodentium* colitis model in which WT and OLFM4<sup>-/-</sup> mice were infected with 1 × 10<sup>8</sup> colony forming units of *C. rodentium* via oral gavage, and their body weight and survival rate were monitored for 7 days (Fig. 2A). Upon *C. rodentium* infection, OLFM4<sup>-/-</sup> mice displayed significantly decreased body weight and increased mortality

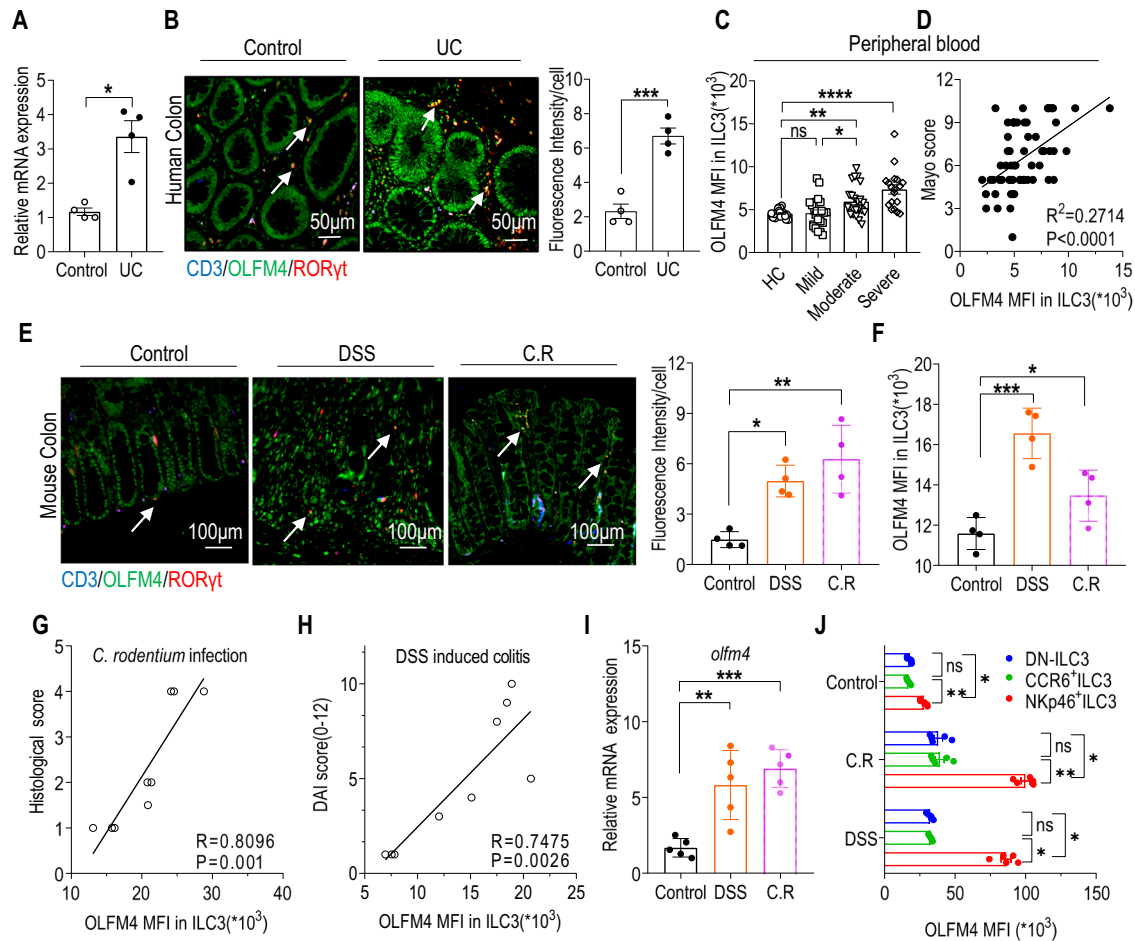


**Fig. 1 | OLFM4 is highly expressed in murine and human intestinal ILC3.**

**A** mRNA expression level of *OLFM4* in mucosal ILC3 of UC patients compared to control ( $n = 4$ ). **B** Immunofluorescence staining of OLFM4 in human colon tissues (left) and statistical results of fluorescence intensity per cell (right). The white arrowhead indicates CD3<sup>+</sup>OLFM4<sup>+</sup>RORγt<sup>+</sup> cells (bar, 50 μm). **C** OLFM4 expression level in ILC3 from peripheral blood of healthy control ( $n = 29$ ), UC patients of mild grade ( $n = 23$ ), moderate grade ( $n = 23$ ) and severe grade ( $n = 18$ ). **D** Correlation analysis of OLFM4 MFI in ILC3 from peripheral blood and Mayo scores in 64 UC patients. **E** Immunofluorescence staining of OLFM4 and RORγt in mouse colon tissue under DSS-induced colitis and *C. rodentium* infection in mice (left) and statistical results of fluorescence intensity per cell (right). The white arrowhead indicates CD3<sup>+</sup>OLFM4<sup>+</sup>RORγt<sup>+</sup> cells (bar, 100 μm). **F** OLFM4 expression levels in ILC3 from colonic LPMCs of DSS-induced colitis, and *C. rodentium* infection mouse

model ( $n = 4$ ). **G** Correlation analysis between OLFM4 MFI in ILC3 of LPMCs and histological scores under *C. rodentium* infection in mice ( $n = 9$ ). **H** Correlation analysis between OLFM4 MFI in ILC3 of LPMCs and DAI (Disease Activity Index) score (0–12) under DSS-induced colitis model ( $n = 9$ ). **I** mRNA level of *Olfm4* in ILC3 sorted from colonic LPMCs of DSS-induced colitis, and *C. rodentium* infection models ( $n = 5$ ). **J** OLFM4 expression levels in ILC3 subsets from colonic LPMCs of *C. rodentium* infection and DSS-induced colitis mouse model ( $n = 5$ ). Data are presented as mean ± SEM, and statistical significance was determined using two-tailed unpaired Student's *t*-tests (**A**, **B**, **E**, **F**, **I**) or one-way ANOVA (**C**, **J**), the relevance of the two variables was measured using correlation analysis (**D**, **G**, **H**). ns, not significant; \* $P < 0.05$ ; \*\* $P < 0.01$ ; \*\*\* $P < 0.001$ . The experiments were performed three times (at least three replicates).

on days 6 and 7 (Fig. 2B, C), in addition to an enlarged spleen (Figs. 2D and S9A). Hematoxylin and eosin (HE) staining revealed increased pathology in OLFM4<sup>-/-</sup> mice, including immune cell infiltration, crypt hyperplasia, and edema (Figs. 2E and S9B). Additionally, OLFM4<sup>-/-</sup> mice exhibited an elevated bacterial burden in the liver and spleen (Fig. 2F, G), while no significant difference was observed in fecal samples compared to control mice (Fig. S9C) than control mice. It has been reported that the deficiency and dysfunction of ILC3 and Th17 cells can lead to intestinal mucosal barrier impairment and severe intestinal inflammation under *C. rodentium* infection<sup>47,48</sup>. We initially assessed proportion and absolute numbers of CD4<sup>+</sup>RORγt<sup>+</sup> cells in both WT and OLFM4<sup>-/-</sup> mice. The results showed that the deficiency of OLFM4 did not exert a significant impact on the alteration of CD4<sup>+</sup>RORγt<sup>+</sup> cells (Fig. 2H). Subsequently, we tested the proportion and absolute number of total ILC3s in LPMCs from the colon and mLN. LPMCs and mLN from OLFM4<sup>-/-</sup> mice exhibited a significantly lower level and numbers of ILC3s than those from WT mice (Figs. 2I and S9D, E). The deficiency of OLFM4, however, did not have an

impact on the distribution of ILC3 subsets such as NKp46<sup>+</sup>ILC3 and CCR6<sup>+</sup>ILC3 (Fig. 2J). Moreover, IL-22-producing ILC3s were markedly reduced in the intestine of OLFM4<sup>-/-</sup> mice (Fig. 2K, L). In contrast, no significant changes were observed in the proportion of IL-17-producing ILC3s (Fig. S9F, G). The effector molecules of IL-22<sup>36,49,50</sup>, such as *RegIIIβ* and *RegIIIγ*, and mucoprotein, *Mucin 1* and tight junction protein, *Claudin 2*, which play a crucial role in forming a bacterial resistance, showed significantly lower expression in OLFM4<sup>-/-</sup> mice than in WT mice (Fig. 2M). This was consistent with published data, IL-22<sup>+</sup> innate cell populations in the gut lamina propria are critical for the response to bacterial infection<sup>51</sup>. Although OLFM4 expression was observed in ILC1s and ILC2s (Fig. S3D, E), their frequency and absolute numbers in mLN (Fig. S10A, B) and LPMCs (Fig. S10C, D) were tested and no significant difference was observed between OLFM4<sup>-/-</sup> and WT mice. Christina Song et al. reported that *Tcrbd*-deficient mice, which lack T cells, can resist bacterial infection through ILC3<sup>52</sup>, which implying that ILC3 was the predominant source of IL-22 and IL-17, and the contribution of CD4<sup>+</sup>T cells to IL-17 and IL-22 was

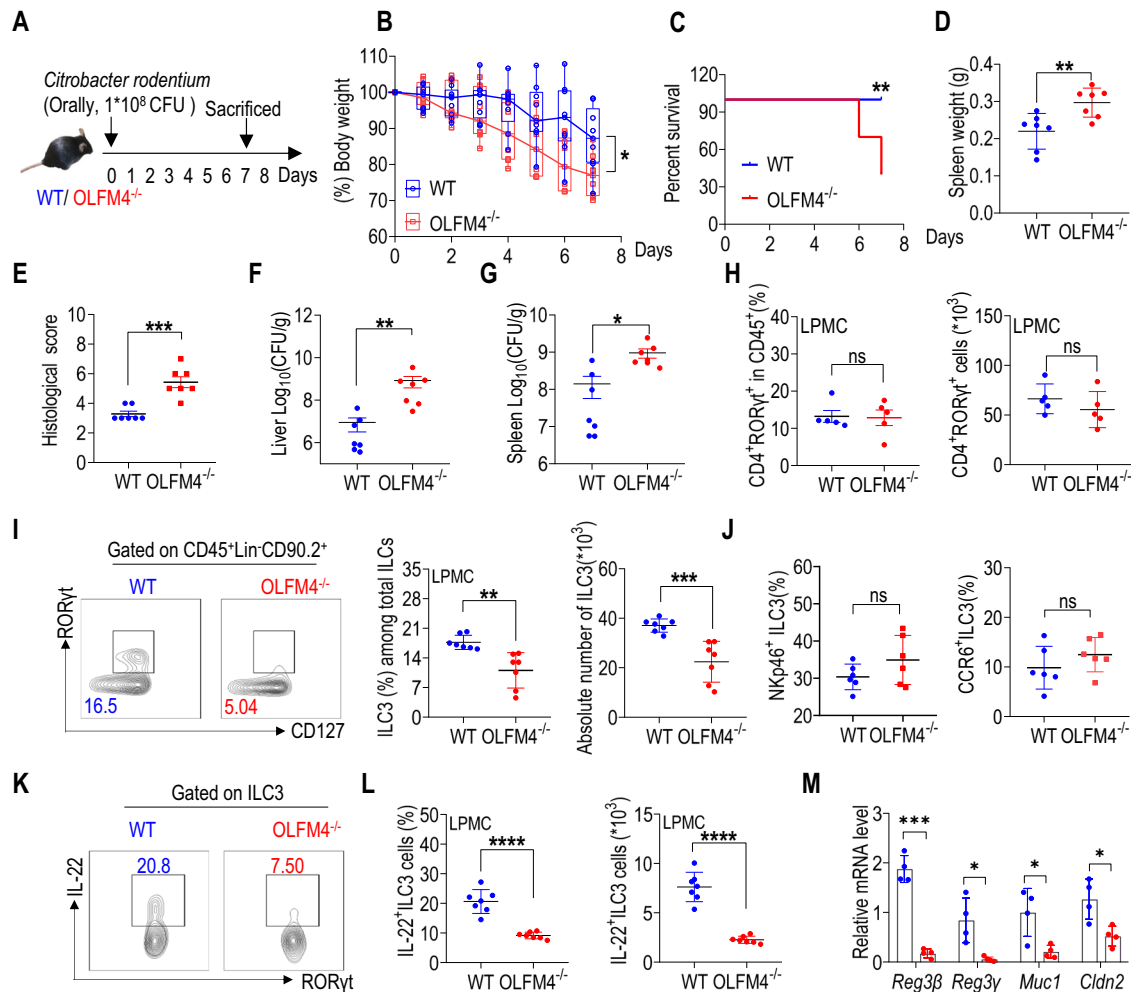


**Fig. 2 | OLFM4 is required for IL-22<sup>+</sup> ILC3s in pathogen resistance.** **A** The experimental scheme of *C. rodentium* infection mouse model. WT and OLFM4<sup>-/-</sup> mice were orally inoculated with 1 × 10<sup>8</sup> CFU of *C. rodentium*. Samples were harvested on day 7 post-infection. **B** Percentage of the initial weight during colitis (n = 9). **C** Comparison of survival rates between indicated mice at 7dpi. **D** Spleen weight of indicated mice after infection (n = 7). **E** Histological score of the colon at 7 dpi (n = 7). Log<sub>10</sub> CFU of *C. rodentium* in (F) liver and (G) spleen (n = 7). **H** Statistical results of proportion and absolute numbers of CD4<sup>+</sup>RORγt<sup>+</sup> cells (n = 5). **I** Representative FACS plots and statistical results of the proportion and absolute numbers of ILC3 in LPMCs from indicated mice (n = 7). **J** Statistical results

of proportion of the of Nkp46 + ILC3 (left) and CCR6 + ILC3 (right) in LPMCs (n = 6). **K** Representative FACS plots of IL-22 expressing ILC3 in LPMCs mice during colitis. **L** Statistical results of proportion and absolute numbers of IL-22-expressing ILC3 (n = 7). **M** mRNA levels of *Reg3b*, *Reg3g*, *Muc1*, and *Cldn2* in colon tissues (n = 4). Data are presented as mean ± SEM, and statistical significance was determined using a two-tailed unpaired Student's *t*-test (**B**, **D**–**J**, **L**, **M**). Kaplan–Meier analysis and survival curves were performed for survival analysis (**C**). ns, not significant; \**P* < 0.05; \*\**P* < 0.01; \*\*\**P* < 0.001. The experiments were performed three times (at least three replicates).

minor at early stage of *C. rodentium*-induced colitis, and our data also confirm this. Above observations suggest that ILC3 may be involved in that OLFM4 deficiency accelerated the onset and severity of the bacterial infection.

To further identify ILC3 dysfunction caused by OLFM4 deficiency, equal numbers of intestinal ILC3 (lineage<sup>-</sup>CD45<sup>low</sup>CD90<sup>high</sup>)<sup>20,53</sup> (Fig. 3A) from WT and OLFM4<sup>-/-</sup> mice were adoptively transferred into Rag2<sup>-/-</sup>IL2rγ<sup>-/-</sup> mice (NCG mice, lacking of T, B, ILCs and NK cells) via tail-vein injections, followed by a model of *C. rodentium*-induced colitis for 7 consecutive days (Fig. 3B). The OLFM4<sup>-/-</sup> ILC3 recipients exhibited increased body weight loss and higher mortality rates than the WT control (Fig. 3C, D). *C. rodentium* infection had little effect on gross pathology in the colons of WT-ILC3-transferred NCG mice, while ILC3-transferred OLFM4-deficient mice had significantly increased histological scores (Fig. 3E), and increased bacterial invasion in the spleen and liver (Fig. 3F, G). Overall, OLFM4 deficiency may play an important protective role in the *C. rodentium* colitis mouse model via IL-22-producing ILC3s.

To unequivocally demonstrate the direct regulation role of OLFM4 in immune cells, mix BM chimera was performed (Fig. 3H). Mixed BM chimeras were generated by mixing BM cells from WT (CD45.1<sup>+</sup>) and WT or OLFM4<sup>-/-</sup> (CD45.2<sup>+</sup>) mice at a 1:1 ratio, followed by transfer into irradiated CD45.1<sup>+</sup> recipients. Recipients were sacrificed five weeks after injection BM cells for further analysis of the expression of CD45.1 and CD45.2 in spleen. WT and OLFM4<sup>-/-</sup> bone marrow cells efficiently repopulated splenocytes at an equal ratio, proving the success of chimaera construction (Fig. S11), proving the success of chimaera construction. Recipients were then infected with 1 × 10<sup>8</sup> colony forming units of *C. rodentium* via oral gavage (Fig. 3H). In line with the observation from OLFM4<sup>-/-</sup> mice, OLFM4<sup>-/-</sup> chimera group exhibited susceptibility to *C. rodentium* infection (Fig. 3I–O), including a more severe weight loss (Fig. 3I), higher mortality rates (Fig. 3J), increased pathology in intestine (Fig. 3K), enlarged spleen (Fig. 3L), elevated bacterial burden in spleen and liver than that in WT chimera group (Fig. 3M, N), along with lower expression of effector molecules of *RegIIIβ* and *RegIIIγ*, while no change of



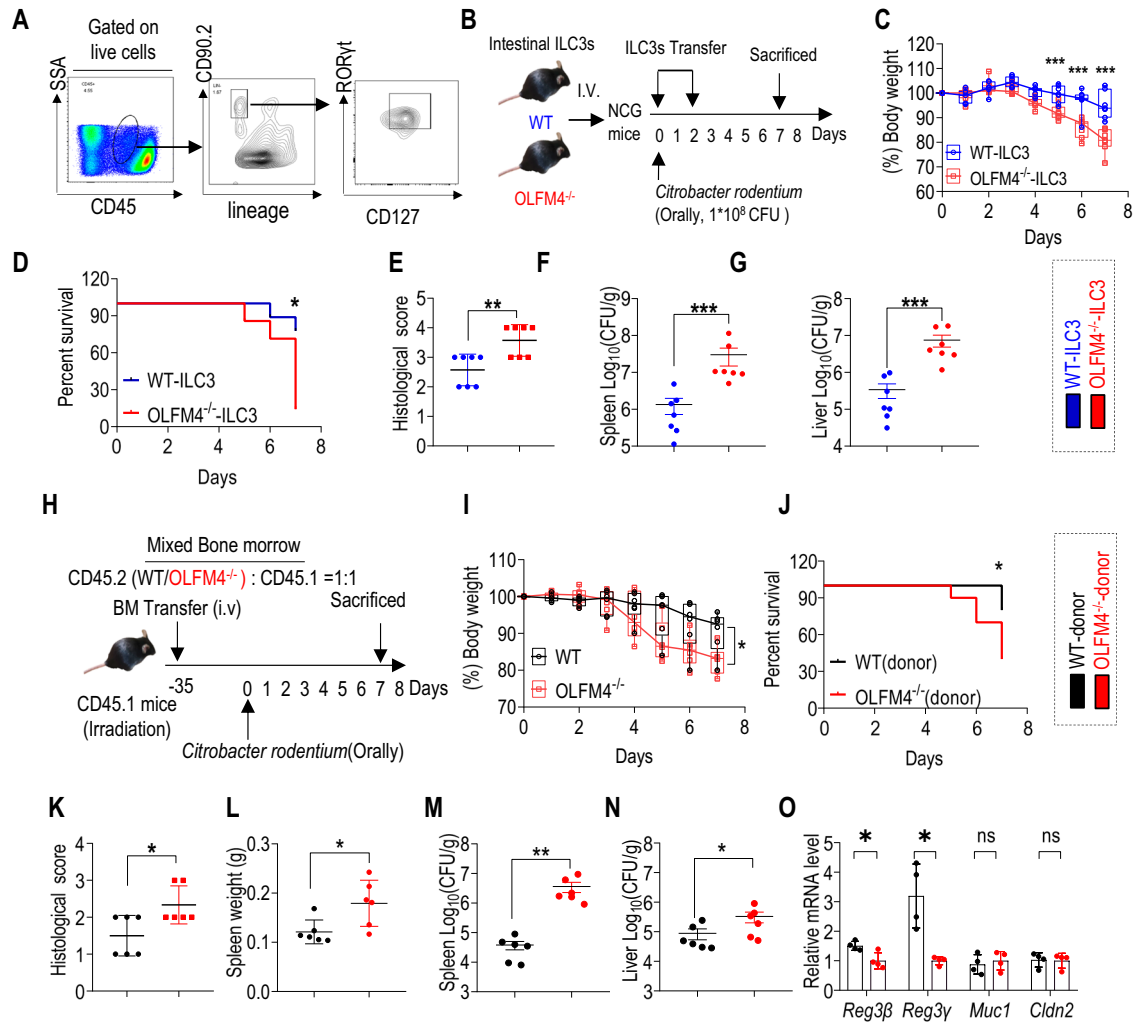


**Fig. 3 | OLFM4 exerts direct effects on the progression of intestinal inflammation by modulating immune cells.** **A** Flow sorting strategy of ILC3. Purified ILC3s (Lineage<sup>-</sup>CD45<sup>low</sup>CD90<sup>high</sup>) from OLFM4<sup>-/-</sup> or WT mice. **B** The experimental scheme. Purified ILC3s were adoptively transferred into Rag2<sup>-/-</sup> Il2rγ<sup>-/-</sup> (NCG) mice at 0 and 2 dpi. NCG mice were orally inoculated with 1 × 10<sup>8</sup> CFU of *C. rodentium*. Samples were harvested on day 7 post-infection. Data are pooled from two independent experiments (n = 7). **C** Body weights of infected mice are plotted as the percentage of initial body weight (n = 7). **D** Survival rates between indicated mice at 7 dpi. **E** Histological score of the colon at 7 dpi (n = 7). **F–G** Pathogen counts in indicated tissues at 7 dpi (n = 7). **H** The experimental scheme of a bone marrow transplantation (BMT) experiment. The bone marrow cells from WT (CD45.2) and OLFM4<sup>-/-</sup> (CD45.2) were mixed in a 1:1 ratio, and 10<sup>7</sup> mixed cells were injected via the tail vein into CD45.1 recipient mice that had been subjected to irradiation

(900 cGy) to deplete their hematopoietic stem cells. After 30 days of hematopoietic reconstruction, mice were orally inoculated with 1 × 10<sup>8</sup> CFU of *C. rodentium*. Samples were harvested on day 7 post-infection. **I** Percentage of the initial weight during colitis (n = 5). **J** Survival rates of indicated mice at 7dpi. **K** Histological score of the colon at 7 dpi (n = 6). **L** Spleen weight of indicated mice after *C. rodentium* infection (n = 6). Log<sub>10</sub> CFU of *C. rodentium* in **(M)** spleen and **(N)** liver (n = 6). **O** mRNA levels of *Reg3b*, *Reg3g*, *Muc1*, and *Cldn2* in colon tissues (n = 4). Data are presented as mean ± SEM, and statistical significance was determined using a two-tailed unpaired Student's *t*-test (C, E–G, I, K–O). Kaplan–Meier analysis and survival curves were performed for survival analysis (D, J). ns, not significant; \**P* < 0.05; \*\**P* < 0.01; \*\*\**P* < 0.001. The experiments were performed three times (at least three replicates).

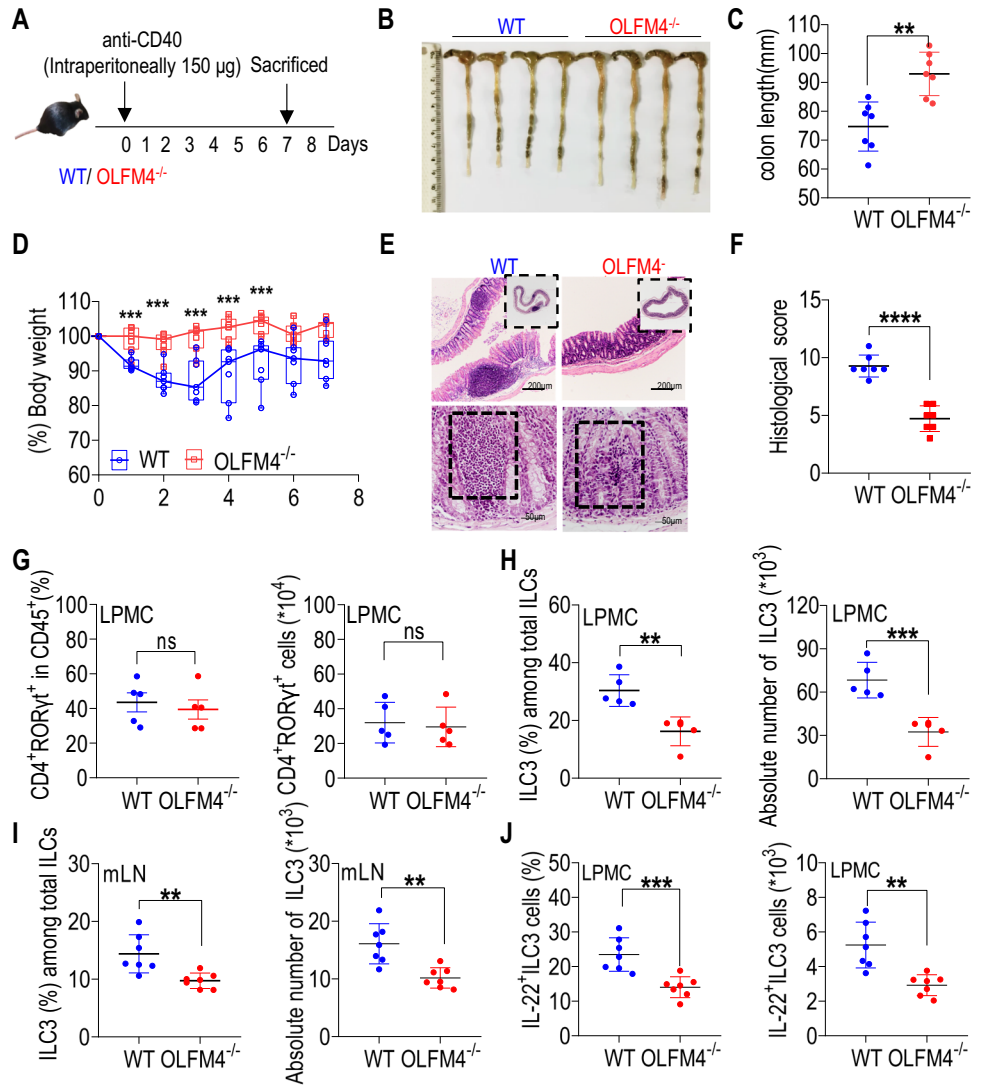
*Muc1* and *Cldn2* (Fig. 3O). Collectively, OLFM4 exerts direct effects on the progression of intestinal inflammation through modulation of immune cells.

**OLFM4 deficiency ameliorates anti-CD40-induced inflammation**  
Anti-CD40 antibody can induce intestinal inflammation through both T cell immunity and innate immunity. The dysregulated activation of ILC3s leads to the development of acute inflammatory and autoimmune diseases, with consequent tissue damage<sup>54</sup>. Excessive production of IL-22 and GM-CSF by ILC3s, rather than IL-17A, induces intestinal inflammation in an anti-CD40 colitis model<sup>28,55</sup>.

To validate these results, an anti-CD40 colitis model was established using OLFM4<sup>-/-</sup> mice (Fig. 4A). WT mice exhibited significantly more

severe clinical symptoms than OLFM4<sup>-/-</sup> mice, as evidenced by shorter colons, increased weight loss, enhanced immune cell infiltration, and a higher histological score in the HE staining results (Fig. 4B–F). Consistent with the previous results, the proportion and number of CD4<sup>+</sup>RORγt<sup>+</sup>T cells indicated no difference between OLFM4<sup>-/-</sup> and WT mice (Fig. 4G). In accordance with previous findings, analysis of the proportion and absolute cell numbers of total ILC3s from LPMCs and mLNs from OLFM4<sup>-/-</sup> mice revealed a lower percentage of ILC3s than in OLFM4<sup>fl/fl</sup> mice (Fig. 4H–I). These results are consistent with previous observations that the loss of ILC3s contributes to protection from anti-CD40-induced inflammation<sup>28</sup>. Furthermore, IL-22<sup>+</sup> ILC3s from the colons of OLFM4<sup>-/-</sup> mice were significantly decreased compared to those in WT mice (Fig. 4J). Collectively, these results suggest that OLFM4 deficiency

**Fig. 4 | OLFM4 deficiency ameliorates inflammation induced by anti-CD40 antibody.** **A** The experimental scheme of anti-CD40 antibody mouse model **(B)** Colitis images and **(C)** colon length of anti-CD40-treated mice ( $n = 7$ ). **D** Weights are shown as a percentage of the initial weight of mice after treatment with anti-CD40 antibody. **E** Representative H&E-stained sections (scale bars: 200  $\mu\text{m}$ , upper; 50  $\mu\text{m}$ , lower) and **(F)** histological scores of the colon from anti-CD40-treated mice ( $n = 7$ ). **G** Statistical results of proportion and absolute numbers of  $\text{CD4}^+\text{ROR}\gamma\text{T}^+$  cells ( $n = 5$ ). **H** statistical results of the proportion and absolute numbers of ILC3 in LPMCs ( $n = 5$ ). **I** Statistical results of the proportion and absolute numbers of ILC3 in mLN ( $n = 7$ ). **J** Statistical results of the proportion and absolute numbers of IL-22-expressing ILC3 ( $n = 7$ ). Data are presented as mean  $\pm$  SEM, and statistical significance was determined using a two-tailed unpaired Student's  $t$ -test (**C**, **D**, **F**–**J**). ns, not significant; \* $P < 0.05$ ; \*\* $P < 0.01$ ; \*\*\* $P < 0.001$ . The experiments were performed three times (at least three replicates).



markedly diminishes the innate immune responses induced by ILC3 during intestinal inflammation. OLFM4 is essential for maintaining the homeostasis of IL-22<sup>+</sup>ILC3 cell numbers and preserving their functional integrity.

**OLFM4 deficiency in RORγT compartment modulates intestinal inflammation through downregulation of ILC3 and IL-22 expression**

To further investigate the role of the OLFM4 in intestinal ILC3s, we generated  $\text{ROR}^{\text{Cre}}\text{OLFM4}^{\text{fl/fl}}$  mice by crossing  $\text{OLFM4}^{\text{fl/fl}}$  mice with  $\text{ROR}^{\text{Cre}}$  mice. Firstly, we assessed OLFM4 expression in ILC3s,  $\text{CD4}^+\text{T}$  cells, epithelial and endothelial cells from the LPMCs of  $\text{OLFM4}^{\text{fl/fl}}$  and  $\text{ROR}^{\text{Cre}}\text{OLFM4}^{\text{fl/fl}}$  mice. Data showed that compared with  $\text{OLFM4}^{\text{fl/fl}}$  mice, a significantly decrease of OLFM4 expression in ILC3 and  $\text{CD4}^+\text{T}$  cells was observed from  $\text{OLFM4}^{\text{fl/fl}}\text{ROR}^{\text{Cre}}$  mice, while no change was indicated of epithelial and endothelial cells from both mice, and validating the deficiency of *olfm4* gene in  $\text{ROR}\gamma\text{T}^+$  cells (Fig. S12). Next, a *C. rodentium* infection model was applied to validate the OLFM4-specific regulatory function in ILC3s. Consistent with observations in  $\text{OLFM4}^{-/-}$  mice infected with *C. rodentium*,  $\text{ROR}^{\text{Cre}}\text{OLFM4}^{\text{fl/fl}}$  mice rapidly lost body weight and exhibited more severe colitis than  $\text{OLFM4}^{\text{fl/fl}}$  mice (Fig. 5A–G). The aggravation of intestinal inflammation in  $\text{ROR}^{\text{Cre}}\text{OLFM4}^{\text{fl/fl}}$  mice was further supported by higher bacterial loads in the spleen and liver, as well as lower expression levels of *RegIIIβ*, *RegIIIγ*, *Muc1*, *Cldn2*. (Fig. 5H). Meanwhile, following anti-CD40-induced colitis,  $\text{ROR}^{\text{Cre}}\text{OLFM4}^{\text{fl/fl}}$  mice exhibited significantly

less severe clinical symptoms than  $\text{OLFM4}^{\text{fl/fl}}$  mice.  $\text{OLFM4}^{\text{fl/fl}}$  mice had a shorter colon length (Fig. 5I, J), higher histological scores (Fig. 5K, L), and exhibited significant weight reduction within a span of 2 to 3 days (Fig. 5M), compared with  $\text{ROR}^{\text{Cre}}\text{OLFM4}^{\text{fl/fl}}$  mice.

In terms of cell phenotypes, both *C. rodentium* infection and anti-CD40 treatment did not significantly alter the proportions and absolute numbers of  $\text{CD4}^+\text{ROR}\gamma\text{T}^+$  cells in  $\text{ROR}^{\text{Cre}}\text{OLFM4}^{\text{fl/fl}}$  mice compared with those in  $\text{OLFM4}^{\text{fl/fl}}$  mice (Fig. 6A, B). On the other hand, it was observed that the frequency and absolute number of ILC3s in LPMCs of  $\text{ROR}^{\text{Cre}}\text{OLFM4}^{\text{fl/fl}}$  mice were significantly lower than those in LPMCs and mLNs of  $\text{OLFM4}^{\text{fl/fl}}$  mice under both colitis models (Figs. 6C, D and S13A, B). The proportion and absolute number of IL-22<sup>+</sup> ILC3s consistently decreased in  $\text{ROR}^{\text{Cre}}\text{OLFM4}^{\text{fl/fl}}$  mice, whereas no change was observed from the distribution of IL-17<sup>+</sup>ILC3s (Figs. 6E, F, and S13C, D), which was consistent with the phenomena observed in  $\text{OLFM4}^{-/-}$  mice. Additionally,  $\text{ROR}^{\text{Cre}}\text{OLFM4}^{\text{fl/fl}}$  mice exhibited no significantly change in proportions of  $\text{NKp46}^+\text{ILC3}$  and  $\text{CCR6}^+\text{ILC3}$  under *C. rodentium* challenge (Fig. S13E) in LPMC.

We then quantified the proliferation and apoptosis of ILC3s through Ki67 and Annexin V staining. The population of  $\text{Ki67}^+\text{ILC3s}$  significantly decreased in both *C. rodentium* infection and anti-CD40-induced colitis model in  $\text{ROR}^{\text{Cre}}\text{OLFM4}^{\text{fl/fl}}$  mice (Fig. 6G, H), whereas no changes were observed in Annexin V<sup>+</sup>ILC3s (Fig. 6I, J). These data indicate that OLFM4 deficiency in ILC3s impairs their function and inhibits their expansion,

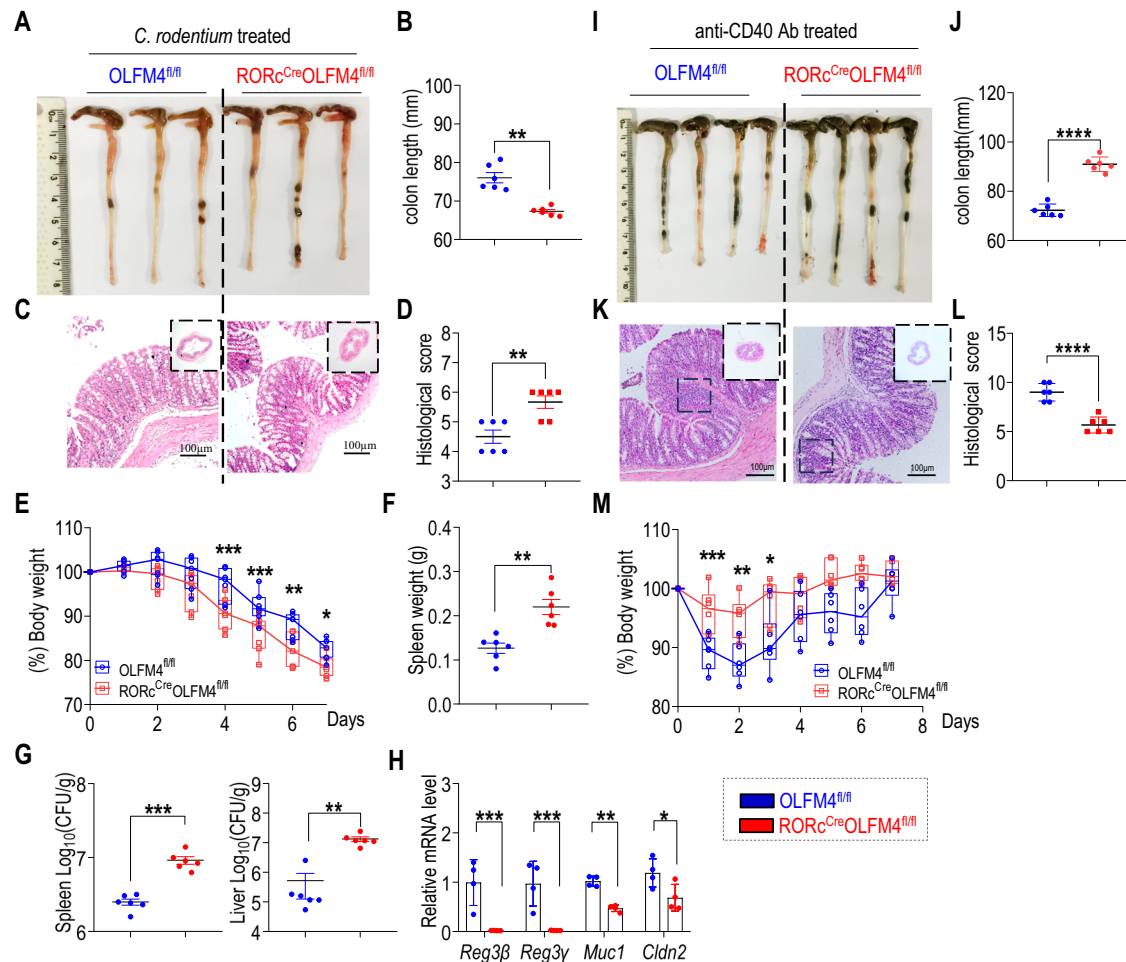


**Fig. 5 | OLFM4<sup>ARORC</sup> mice modulates intestinal inflammation.** **A** Representative colitis images and **(B)** colon lengths of OLFM4<sup>fl/fl</sup> and OLFM4<sup>ARORC</sup> mice under *C. rodentium* infection ( $n = 6$ ). **C** Representative H&E-stained sections (bars: 100  $\mu\text{m}$ ) of the colon. **D** Colonic histopathology scores at 7 dpi ( $n = 6$ ). **E** Weights are shown as a percentage of the initial weight of mice ( $n = 6$ ). **F** Statistical results of spleen weights at 7 dpi ( $n = 6$ ). **G** Log<sub>10</sub> CFU of *C. rodentium* in spleen and liver tissues ( $n = 6$ ). **H** mRNA levels of *Reg3b*, *Reg3g*, *Muc1* and *Cldn2* in colon tissues from indicated mice ( $n = 4$ ). **I** Colitis images and **(J)** colon length of anti-CD40-treated indicated

mice ( $n = 6$ ). **K** Representative H&E-stained sections (scale bars: 100  $\mu\text{m}$ ) and **(L)** histological scores of the colon from anti-CD40-treated indicated mice ( $n = 6$ ). **M** Weights are shown as a percentage of the initial weight of indicated mice after treatment with anti-CD40 antibody. Data are presented as mean  $\pm$  SEM, and statistical significance was determined using a two-tailed unpaired Student's *t*-test (**B**, **D**, **E**–**H**, **J**, **L**, **M**). ns, not significant; \* $P < 0.05$ ; \*\* $P < 0.01$ ; \*\*\* $P < 0.001$ . The experiments were performed three times (at least three replicates).

aggravating bacterial infection-induced acute colitis and resistance to the innate immune responses of ILC3s.

#### OLFM4 promotes ROR $\gamma$ t and IL-22 expression via the ASK1/p38 signaling pathway

P38 MAPK signaling pathways are important in IL-23-mediated IL-22 production in ILC3s<sup>56</sup>. ASK1 is a mitogen-activated protein 3-kinase that is implicated in various cellular functions. ASK1-dependent p38 MAPK signaling is required for innate immunity and pathogen resistance<sup>57</sup>. Phosphorylated ASK1 at Ser845 and dephosphorylated ASK1 at Ser967 or Ser83 can increase ASK activity<sup>58–60</sup> and subsequently activate p38 MAPK. Additionally, ASK1 deficiency increases the susceptibility to colonic inflammation in DSS- or *C. rodentium* induced colitis models<sup>61</sup>. Therefore, we explored whether ASK1 and p38 play a role in the regulation of ILC3 function by OLFM4 in colitis. The phosphorylation levels of both ASK1 (Ser967) and p38 (Thr180/Tyr182) were investigated in the RORc<sup>Cre</sup>OLFM4<sup>fl/fl</sup> and OLFM4<sup>fl/fl</sup> groups under *C. rodentium*-induced colitis. Compared to that in the OLFM4<sup>fl/fl</sup> group, the phosphorylation level of p38 was significantly decreased in the RORc<sup>Cre</sup>OLFM4<sup>fl/fl</sup> group, together with a significant increase in the phosphorylation of ASK1 (Fig. 7A, B).

These results indicate that the ASK1-p38 pathway potentially affects the regulation of ILC3 by OLFM4.

Therefore, to further elucidate the mechanisms by which OLFM4 regulates ILC3 function, we used the MNK3 ILC3 cell line<sup>62</sup>, which is an effective cell model for studying ILC3s<sup>63,64</sup>, and expresses ROR $\gamma$ t and produces high levels of IL-22 and IL-17 in response to IL-23 and IL-1 $\beta$  stimulation. Same to the human and mouse data, OLFM4 was highly expressed in MNK3 cells compared to that in bone marrow cells that also highly expressed OLFM4 (Fig. S14A). Subsequently, to determine the relationship between OLFM4 and ILC3 function, MNK3 cells were transfected with small interfering RNA (siRNA) specific for OLFM4 (si-OLFM4). We first tested the OLFM4 expression level after knockdown of the gene encoding OLFM4 and found a significant reduction in the expression of OLFM4 in MNK3 cells transfected with si-OLFM4 at both the protein and mRNA levels compared to that in the control (Fig. S14B–D). Consistent with the results in the colitis model, there was a corresponding decrease in the phosphorylation of p38, accompanied by a decrease in OLFM4 expression (Figs. 7C and S14E). Moreover, the expression levels of ROR $\gamma$ t in MNK3 cells decreased (Figs. 7D and S14F), and the concentration of IL-22 in the supernatants (Fig. 7E) in MNK3 cells transfected with si-

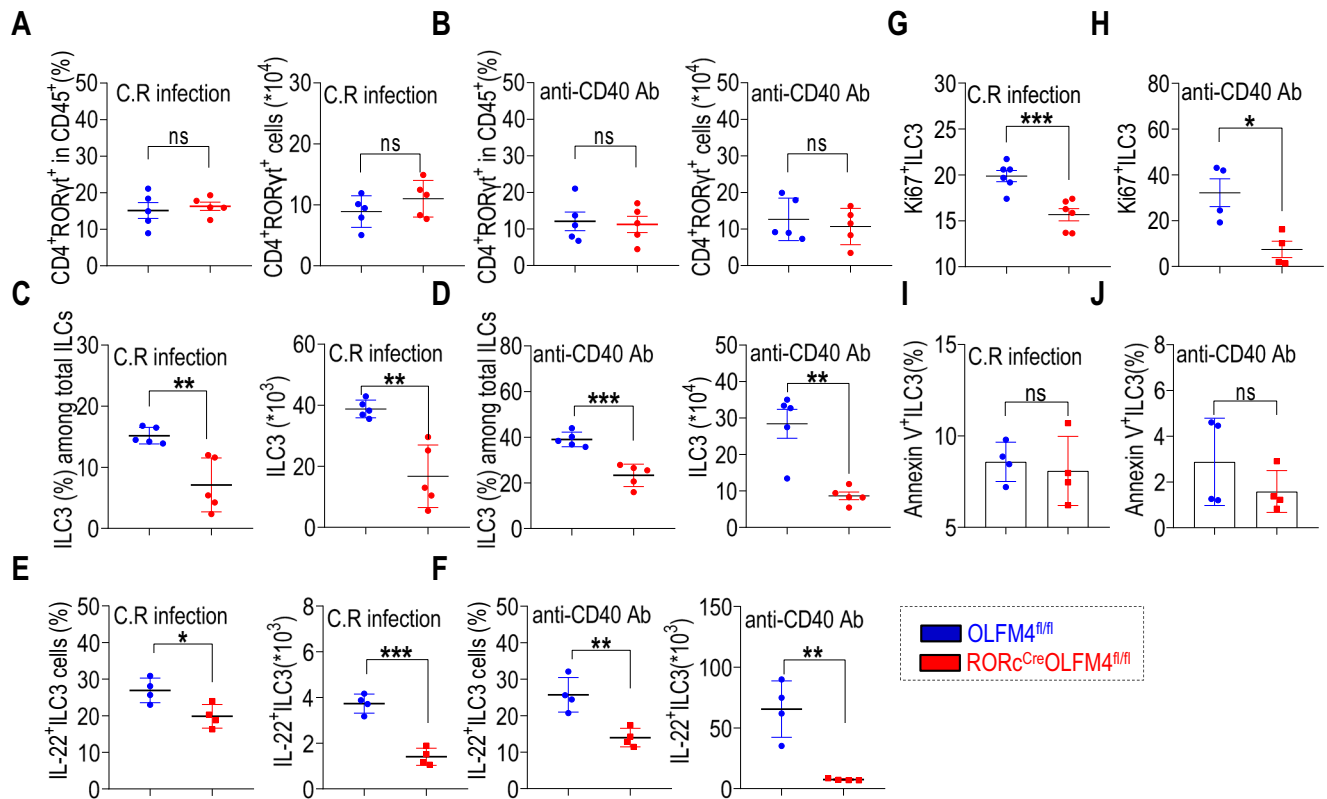


**Fig. 6 | OLFM4<sup>ARORC</sup> mice decreases the amount of ILC3 and IL-22 production.** Statistical results of proportion and absolute numbers of CD4<sup>+</sup>RORγt<sup>+</sup> cells under (A) *C. rodentium* infection ( $n = 5$ ) and (B) anti-CD40 antibody-induced colitis ( $n = 5$ ). Statistical results of the proportion and absolute numbers of ILC3 in LPMCs under (C) *C. rodentium* infection ( $n = 4$ ) and (D) anti-CD40 antibody-induced colitis ( $n = 5$ ). Statistical results of the proportion and absolute numbers of IL-22-expressing ILC3 in (E) *C. rodentium* infected mice ( $n = 4$ ) and (F) anti-CD40-treated mice ( $n = 4$ ). The proportion of Ki67<sup>+</sup>ILC3 in LPMCs from (G) *C. rodentium*

infected mice ( $n = 6$ ) and (H) anti-CD40-treated mice ( $n = 4$ ). The proportion of Annexin V<sup>+</sup>ILC3 in LPMCs under (I) *C. rodentium* infection ( $n = 4$ ) and (J) anti-CD40 induced colitis ( $n = 4$ ). Data are presented as mean  $\pm$  SEM, and statistical significance was determined using a two-tailed unpaired Student's *t*-test (A–J). ns, not significant; \* $P < 0.05$ ; \*\* $P < 0.01$ ; \*\*\* $P < 0.001$ . The experiments were performed three times (at least three replicates).

OLFM4 was lower than that in the control. However, no change of IL-17 production in the supernatants was observed (Fig. S14G). Additionally, the expression of genes associated with ILC3 function, such as *Il23r*, *Ccr6*, *Ncr1*, and *Il22*, was significantly reduced (Fig. 7F).

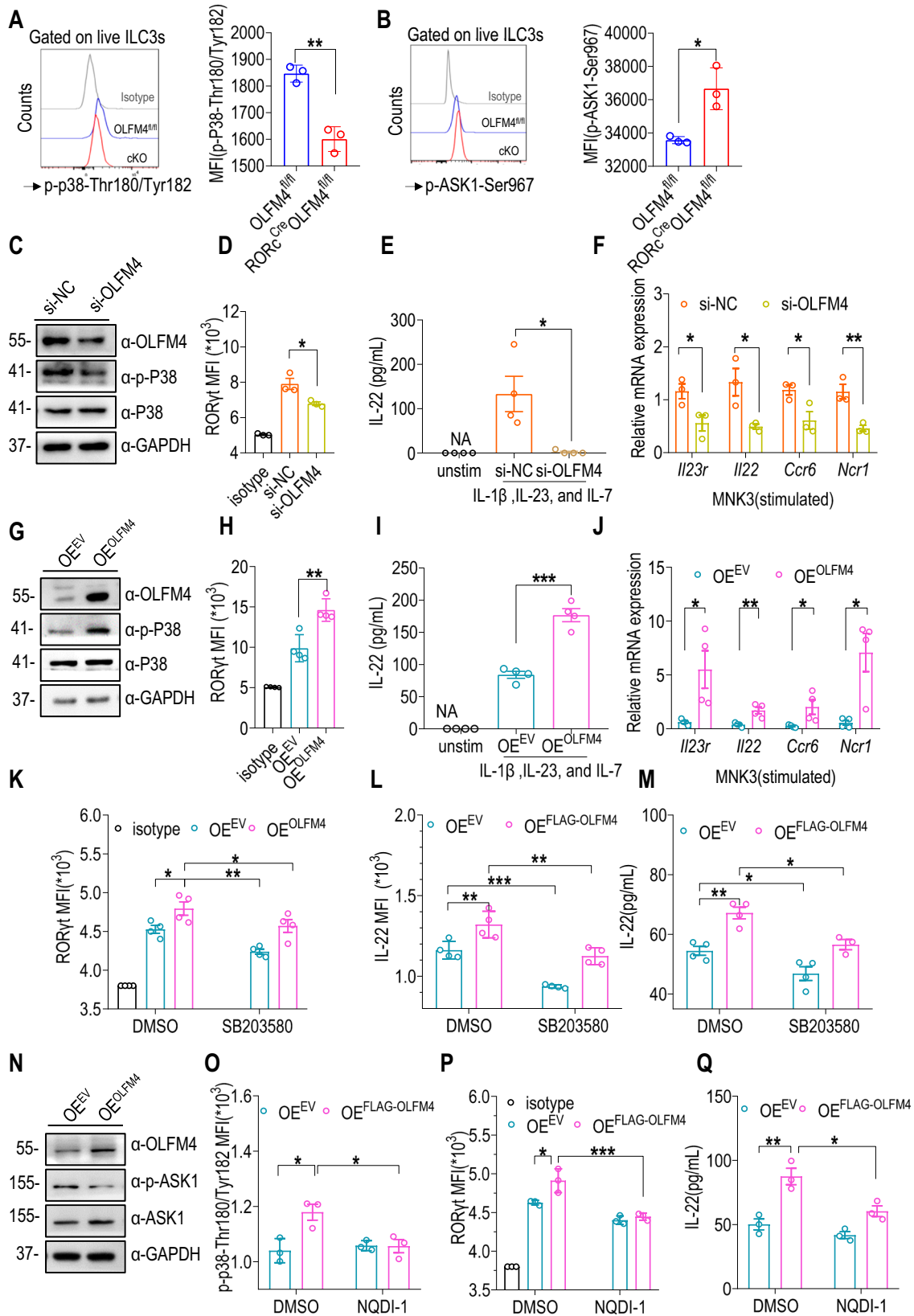
We evaluated the effects of OLFM4 overexpression in MNK3 cells. Higher OLFM4 expression was observed in MNK3 cells transfected with a plasmid encoding OLFM4 (OE<sup>OLFM4</sup>) at both the protein and RNA levels (Fig. S15A–C). Additionally, an increase in p38 phosphorylation (Figs. 7G and S15D), RORγt protein levels (Figs. 7H and S15E), and IL-22 production (Fig. 7I), but not IL-17 production (Fig. S15F–H), was observed. Furthermore, quantitative polymerase chain reaction (qPCR) showed that a series of genes associated with ILC3 function (*Il23r*, *Ccr6*, *Ncr1*, and *Il22*) were significantly upregulated in MNK3 cells transfected with OE<sup>OLFM4</sup> (Fig. 7J).

To determine the specificity of OLFM4-p38 signaling, the p38 inhibitor SB203580 (10  $\mu$ M) was used. Consistent with previous studies, we observed that SB203580 reduced IL-22 production and RORγt expression<sup>65,66</sup>. Overexpression of OLFM4 in MNK3 cells combined with SB203580 significantly reduced the protein level of RORγt compared with that in the overexpressed OLFM4 group (Figs. 7K and S16A). Furthermore, overexpression of OLFM4 in MNK3 cells combined with SB203580 substantially reduced the proportion of IL-22 in MNK3 cells and the concentrations of IL-22 in the supernatants compared to that in the overexpressed OLFM4 group (Figs. 7L, M and S16B). Like the mouse data, overexpression of OLFM4 in MNK3 cells did not affect the proportion of IL-17, and no difference was observed in IL-17 production compared to that in MNK3 cells treated with SB203580 overexpressing OLFM4 (Fig. S16C).

Further examination showed that OLFM4 overexpression resulted in a decrease in the phosphorylation of ASK1 (dephosphorylated ASK1 at Ser967), which in turn resulted in activating of ASK1 and ASK1-mediated activation of p38 pathways in MNK3 cells (Fig. 7N). To verify the specificity of the effects of ASK1 on OLFM4-p38 MAPK signaling, we used a specific inhibitor of ASK1, NQDI-1. Like the p38 inhibitor, NQDI-1 also suppresses OLFM4 function in the regulation of p38-RORγt-IL22 (Figs. 7O–Q and S16D, E). Furthermore, we investigated the effect of ASK1 knockdown by siRNA on the regulation of p38-RORγt-IL22 and observed the same effect on OLFM4 function (Fig. S17A–C).

To further confirm the effects of ASK1-p38 signaling on ILC3 regulation in mice, we used the *C. rodentium* infection model with WT mice and administered daily ASK1 (NQDI-1) or p38 inhibitor (SB203580) treatments, followed by subsequent analysis after 7 days (Fig. 8A). Consistent with observations in *C. rodentium* infected RORC<sup>Cre</sup>OLFM4<sup>fl/fl</sup> mice, *C. rodentium* infected mice with both inhibitors (NQDI-1 and SB203580) treatments exhibited exacerbated intestinal inflammation. Specifically, a substantial decrease in body weight starting from day 4 post *C. rodentium* infection (Fig. 8B), while the spleen weight and the bacterial load in the spleens presented a significant increase (Fig. 8C, D). The colonic pathological score was also elevated (Fig. 8E, F). Additionally, the expression level of *RegIII $\beta$* , *RegIII $\gamma$* , *Muc1* and *Cldn2* was markedly reduced (Fig. 8G), indicating exacerbated intestinal inflammation. In term of cell phenotype, a decrease in the proportion and number of intestine ILC3s





with inhibitor treatment (Fig. 8H, I). As well as a substantial reduction in both the proportions and absolute numbers of IL-22<sup>+</sup>ILC3s and IL-17<sup>+</sup>ILC3s in intestine (Fig. 8J–M). Collectively, our findings suggest that ASK1-p38 signaling downstream of OLFM4 is involved in regulating ILC3 during colitis.

**OLFM4-MTDH complex upregulated by ASK1-p38 MAPK-RORγt signaling is required for functional activation of ILC3s**

OLFM4 is a glycoprotein and has been reported to be expressed on the cell membrane and mitochondria<sup>31,46,67,68</sup>. Additionally, it functions as a secreted protein that is released into the extracellular matrix<sup>67,69</sup>. Thus, proteins that

**Fig. 7 | OLFM4 promotes ROR $\gamma$ t and IL-22 expression through ASK1-p38 MAPK pathway.** **A** MFI of p-p38-Thr180/Tyr182 and **(B)** p-ASK1-Ser967 in ILC3 from *C. rodentium* infected mice was analyzed by flow cytometry ( $n = 3$ ). **C** p38 phosphorylation level (Thr180/Tyr182) in MNK3 cells after transfection with si-OLFM4. **D** Expression level of ROR $\gamma$ t in indicated MNK3 cells ( $n = 3$ ). **E** The secretion level of IL-22 in the culture supernatant stimulated (IL-1 $\beta$ , IL-23, and IL-7) for 48 h ( $n = 4$ ). **F** mRNA levels of *Il23r*, *Il22*, *Ccr6*, and *Ncr1* in stimulated indicated MNK3 cells ( $n = 3$ ). **G** Western blotting of the phosphorylation level of p38 in MNK3 cells after transfected with plasmids encoding OLFM4 (OE<sup>OLFM4</sup>) and empty vector (OE<sup>EV</sup>). **H** ROR $\gamma$ t expression level in stimulated MNK3 cells after overexpression of OLFM4 ( $n = 4$ ). **I** Secretion level of IL-22 in culture supernatant ( $n = 4$ ). **J** mRNA levels of *Il23r*, *Il22*, *Ccr6*, and *Ncr1* in stimulated indicated MNK3 cells ( $n = 4$ ).

Expression levels of **(K)** ROR $\gamma$ t and **(L)** IL-22 in stimulated indicated MNK3 cells after treated with SB203580 or DMSO ( $n = 4$ ). **M** Secretion level of IL-22 in the culture supernatant ( $n = 4$ ). **N** Western blotting of ASK1 phosphorylation level in MNK3 cells after overexpression of OLFM4. Expression levels of **(O)** p-p38-Thr180/Tyr182 and **(P)** ROR $\gamma$ t in stimulated MNK3 cells after overexpression of OLFM4 and treated with NQDI-1 ( $n = 3$ ). **Q** Secretion level of IL-22 in the culture supernatant of indicated MNK3 cells ( $n = 3$ ). Data are presented as mean  $\pm$  SEM, and statistical significance was determined using two-tailed unpaired Student's *t* test (**A, B, D–F, H–J**), or two-way ANOVA (**K–M, O–Q**). ns, not significant; \* $P < 0.05$ ; \*\* $P < 0.01$ ; \*\*\* $P < 0.001$ . The experiments were performed three times (at least three replicates).

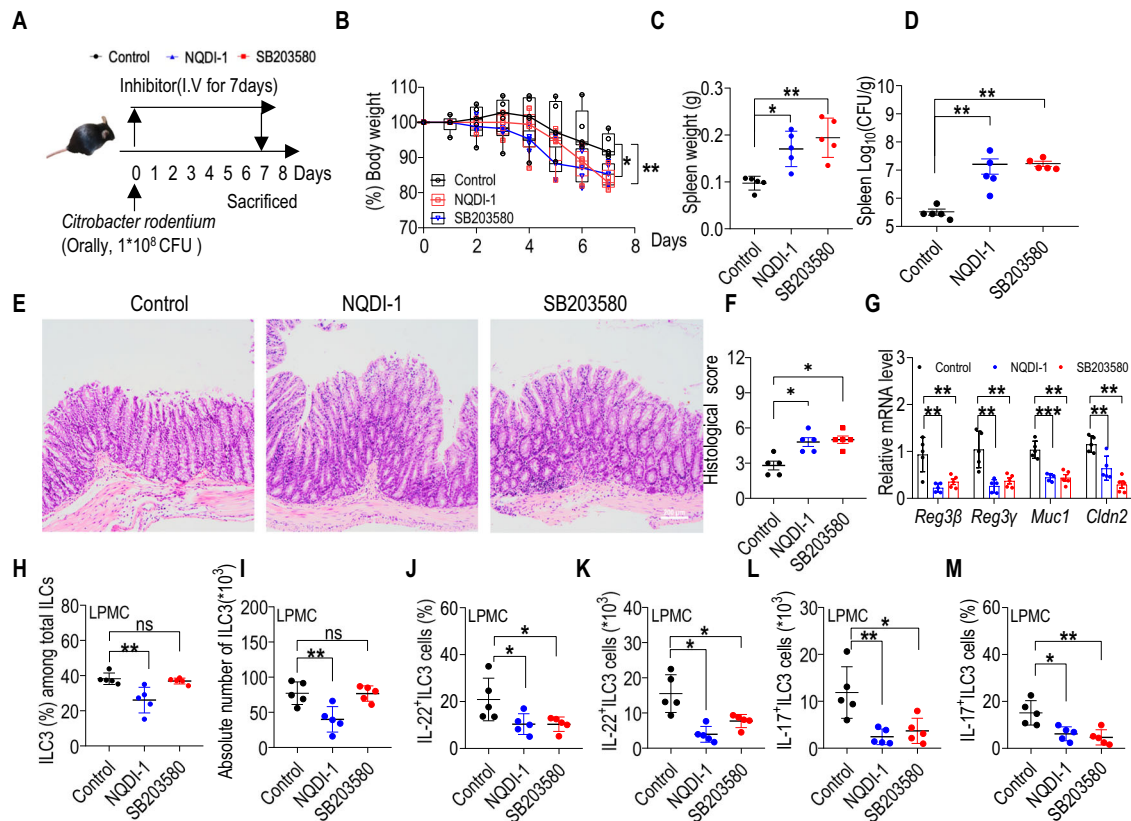


**Fig. 8 | Inhibition of ASK1-P38 pathway led to a substantial reduction in IL22<sup>+</sup> ILC3 cells.** **A** The WT mice were orally administered  $1 \times 10^8$  CFU of *C. rodentium* and treated with or without NQDI-1 or SB203580 daily. Mouse tissues were collected on Day 7 post-infection. **B** Percentage of the initial weight during colitis. **C** Comparison of spleen weight of indicated mice after infection ( $n = 5$ ). **D** Log<sub>10</sub> CFU of *C. rodentium* in spleen ( $n = 5$ ). **E** Representative H&E-stained sections (bars: 200  $\mu$ m) of the colon. **F** Colonic histopathology scores at 7dpi ( $n = 5$ ). **G** mRNA levels of *Reg3b*, *Reg3g*, *Muc1*, and *Cldn2* in colon tissues ( $n = 5$ ). Statistical results of the **(H)** proportion and **(I)** absolute numbers of ILC3 in LPMCs from

indicated mice ( $n = 5$ ). Statistical results of **(J)** proportion and **(K)** absolute numbers of IL-22-expressing ILC3 in LPMCs from indicated mice ( $n = 5$ ). Statistical results of **(L)** proportion and **(M)** absolute numbers of IL-17-expressing ILC3 in LPMCs from indicated mice ( $n = 5$ ). Data are presented as mean  $\pm$  SEM, and statistical significance was determined using a two-tailed unpaired Student's *t*-test (**B–D, F–M**). ns, not significant; \* $P < 0.05$ ; \*\* $P < 0.01$ ; \*\*\* $P < 0.001$ . The experiments were performed three times (at least three replicates).

are highly expressed on the cell membrane of MNK3 and interact with OLFM4 need to be further explored. Immunoprecipitation-mass spectrometry revealed that the MTDH (referred to as AEG-1/LYRIC) from MNK3 ILC3 cell membrane protein affected tumor growth and development, evasion of apoptosis, and had a strong binding affinity for OLFM4 (Fig. S18A–E). Recent studies have shown that MTDH expression in macrophages from the colonic lamina propria is positively correlated with inflammatory colitis severity<sup>70</sup>. MTDH is also a potent modulator of apoptosis via the activation of the p38-MAPK-dependent pathway<sup>71</sup>. Herein, both OLFM4 and MTDH expression level in inflammatory colitis and MNK3 cells were firstly evaluated, and a significantly increased expression was observed from both MTDH and OLFM4 in inflamed

intestinal ILC3s and stimulated MNK3 cells (Fig. S19A, B). And both proteins were localized in the extranuclear region (Fig. S19C). Consistent with the data of OLFM4 expression in humans ILC3s, a substantial increase in MTDH expression in ILC3s of human PBMC from patients with UC compared to healthy controls, and expression of both protein exhibits a positive correlation (Fig. S20A, B). Moreover, MTDH and OLFM4 colocalized in the cytoplasm in intestinal mucosal tissue from UC patients (Fig. S20C). Subsequently, we validated the relationship between OLFM4 and MTDH expression. A glutathione S-transferase (GST) pull-down assay revealed a direct interaction between OLFM4 and MTDH in vitro (Fig. 9A). To measure the binding affinity between OLFM4 and MTDH, we performed a surface plasmon resonance imaging profiling assay and obtained a

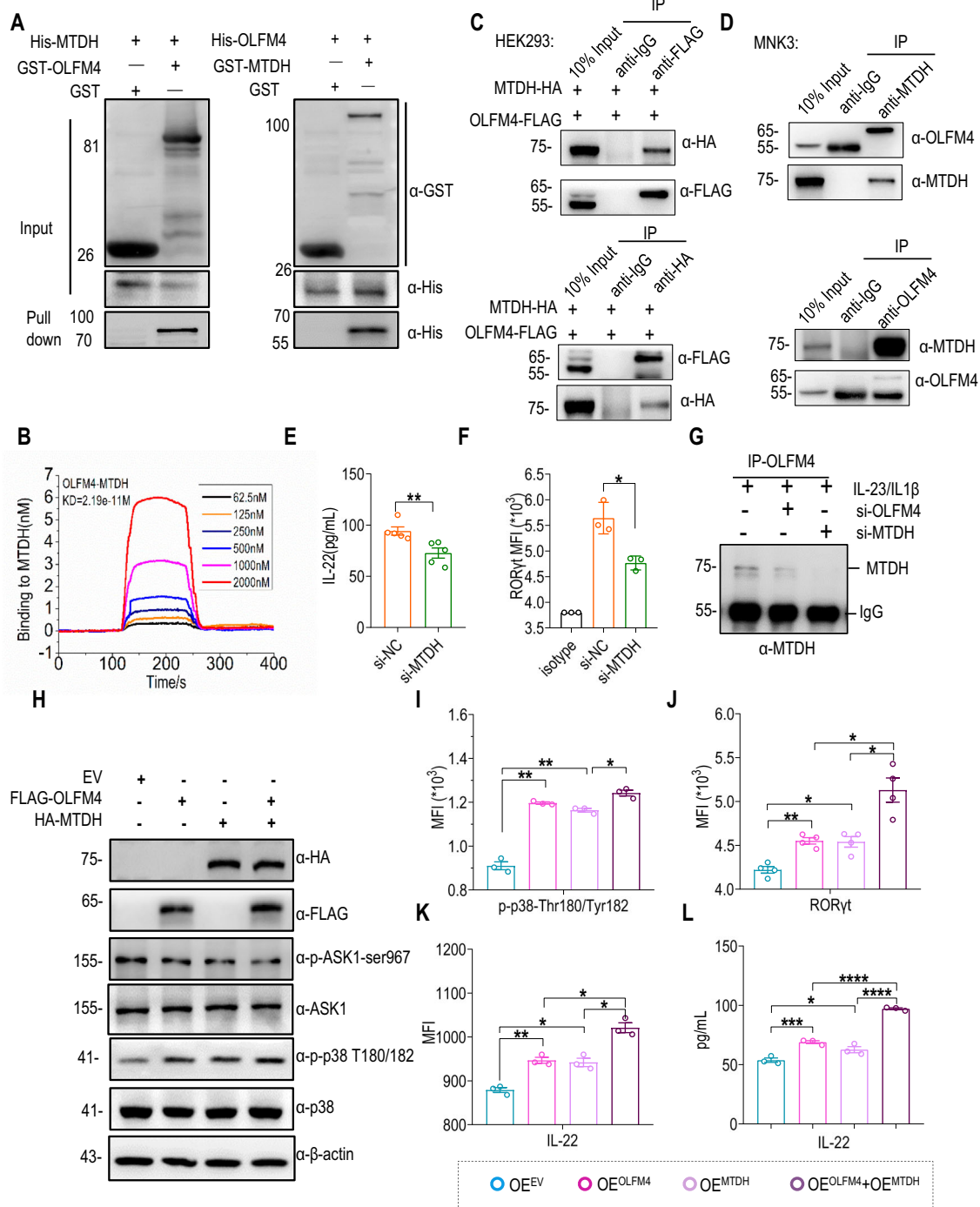


**Fig. 9 | OLFM4-MTDH complex upregulated p38/RORyt signaling is required for functional activation of ILC3s.** **A** Direct association of exogenous OLFM4 with exogenous metadherin (MTDH). **B** Surface plasmon resonance (SPR) affinity measurements of OLFM4 to the immobilized extracellular domain of MTDH. Dissociation constant (KD) values were calculated by software. **C** Immunoprecipitations were performed on HEK293 transfected with plasmids encoding OLFM4 and MTDH. **D** Immunoprecipitations were performed on MNK3 lysates. **E** Secreted level of IL-22 in the culture supernatant ( $n = 5$ ). **F** RORyt expression level in stimulated MNK3 cells ( $n = 3$ ). **G** Immunoprecipitations were

performed on MNK3 transfected with siOLFM4 or siMTDH. **H** Western blotting of p38 phosphorylation level and ASK1 phosphorylation level in MNK3 cells. Expression levels of (**I**) p-p38-Thr180/Tyr182 ( $n = 3$ ), (**J**) RORyt ( $n = 4$ ), and (**K**) IL-22 ( $n = 3$ ) in stimulated MNK3 cells ( $n = 3$ ). **L** Secreted level of IL-22 in the culture supernatant ( $n = 3$ ). Data are presented as mean  $\pm$  SEM, and statistical significance was determined using two-tailed unpaired Student's  $t$  test (**E**, **F**), or two-way ANOVA (**I**–**L**). ns, not significant; \* $P < 0.05$ ; \*\* $P < 0.01$ ; \*\*\* $P < 0.001$ . The experiments were performed three times (at least three replicates).

dissociation KD value of  $2.19 \times 10^{-11}$  M for the two proteins (Fig. 9B), suggesting a strong direct interaction between them. To further substantiate the OLFM4-MTDH interaction in cells, we constructed a panel expressing FLAG-tagged OLFM4 and hemagglutinin (HA)-tagged MTDH. Plasmid pairs were co-transfected into human embryonic kidney (HEK) 293 T cells.

In agreement with the GST pull-down data, a Co-IP assay confirmed that Flag-OLFM4 interacted with HA-MTDH in HEK 293 T cells (Fig. 9C), which was verified by protein-protein interactions in vivo in MNK3 cells (Fig. 9D). These findings indicated that OLFM4 directly binds to MTDH in cytoplasm.

The ASK1-p38-ROR $\gamma$ t signaling pathway is critical for ILC3 function which is regulated by OLFM4. Subsequently, we explored the role of the OLFM4-MTDH complex in activating the ASK1-p38-ROR $\gamma$ t-IL-22 signaling pathway. Consistent with the OLFM4 data, knockdown of MTDH in MNK3 cells decreased the expression of IL-22 and ROR $\gamma$ t (Figs. 9E, F and S21A, B) but did not affect IL-17 level (Fig. S21C). Moreover, knockdown of OLFM4 or MTDH led to a reduction in their combination (Fig. 9G). Using a previous panel expressing FLAG-tagged OLFM4 and HA-tagged MTDH, the plasmid pairs were co-transfected into MNK3 cells. We observed that, when compared with only overexpressed OLFM4 or MTDH, co-overexpression of OLFM4 and MTDH resulted in a decrease in the phosphorylation of ASK1 (dephosphorylated ASK1 at Ser967), which resulted in an increase in ASK1 activity and a further increase in p38 phosphorylation (Figs. 9H, I and S22A, B), along with increased ROR $\gamma$ t expression, IL-22 expression and production in the supernatants (Figs. 9J–L and S23A–C). However, no changes in IL-17 expression were observed (Fig. S23D, E). These data suggest that the OLFM4-MTDH complex enhances the expression of ROR $\gamma$ t and its downstream effector molecule IL-22 via the ASK1-p38 pathway. Collectively, these results suggest that the OLFM4/MTDH-ASK1-p38 MAPK axis mediates the activation of ILC3 function.

## Discussion

Here, we demonstrated that OLFM4 protects the intestine from acute pathogen-induced inflammation via IL-22-producing-ILC3s. OLFM4 deficiency also relieved anti-CD40-induced inflammation caused by the dysregulated activation of ILC3s. Therefore, as a vital positive regulator of ILC3 function, OLFM4 plays a role in the IL-22<sup>+</sup>ILC3 population under different conditions of intestinal inflammation. These findings also demonstrated the involvement of ASK1-p38-ROR $\gamma$ t signaling in the regulation of IL-22<sup>+</sup>ILC3s by OLFM4 and the necessity of the OLFM4-MTDH complex-mediated upregulation of ASK1/p38/ROR $\gamma$ t signaling for the activation of IL-22<sup>+</sup>ILC3s (Fig. S24). Thus, our findings identified OLFM4 as a new regulator of IL-22<sup>+</sup>ILC3s and showed that OLFM4 contributes to the regulation of ILC3-mediated inflammation.

ILC3s play a key role in regulating gastrointestinal health through several pathways, including the activation of IECs to produce AMPs to eliminate pathogens, promote epithelial cell regeneration to accelerate tissue repair, and regulate adaptive immune homeostasis<sup>72</sup>. IL-22-producing-ILC3s play an important role in maintaining the stability of the gut microbiota and regulating inflammation<sup>73</sup>. IL-22 can induce epithelial cell proliferation and survival and promote tissue repair. However, excess IL-22 induces the production of neutrophil chemokines by epithelial cells, leading to neutrophil accumulation and tissue destruction<sup>74</sup>. Two animal models, *C. rodentium* infection and anti-CD40-induced innate colitis used in our study revealed the distinctive characteristics of IL-22<sup>+</sup>ILC3s. In the *C. rodentium* infection model, an anti-bacterial response initiates by inducing antigen-presenting cells to secrete cytokines IL-23/IL-1 $\beta$  upon bacterial infection, resembling acute colitis without severe autoimmune inflammatory damage caused by neutrophil accumulation. However, absence of ILC3 results in severe bacterial infection of intestinal tissue, depletion of secretory cells and goblet cells, and further inflammatory responses. Therefore, promoting the activity of ILC3, particularly NCR<sup>+</sup>ILC3 (NKp46<sup>+</sup>ILC3), is beneficial for intestinal antibacterial activity and mucosal repair during treatment of infectious acute enteritis in humans. In anti-CD40 antibody induced model, anti-CD40 antibodies primarily activate dendritic cells (DCs) to enhance the expression and secretion of IL-23, resulting in excessive activation of ILC3. This process leads to a substantial release of cytokines such as IL-22, IL-17, and GM-CSF by ILC3, triggering massive neutrophil accumulation and the release of pro-inflammatory factors like IL-6 and TNF- $\alpha$ , thereby causing inflammatory damage to the intestine<sup>75</sup>. Additionally, NCR<sup>+</sup>ILC3 undergo transformation into NCR ILC3 and ILC1 subtypes while secreting significant amounts of IL-17 and IFN- $\gamma$ , further exacerbating intestinal mucosal damage<sup>76–78</sup>. Previous studies have reported increased expression levels of CD40L and CD40 in both bloodstream and intestinal mucosa of

patients with inflammatory bowel disease (IBD). Moreover, CD40 receptors are highly overexpressed in the mucosa and subepithelial layer components within inflamed intestines, showing correlation with clinical activity in ulcerative colitis (UC). Therefore, neutrophil aggregation induced by CD40 antibody more closely resembles autoimmune hyperactivation leading to intestinal damage observed in human IBD cases. To sum up, IL-22 plays a pivotal role in both models, with its deficiency or excessive secretion potentially triggering disease onset.

In our study, we found that OLFM4-deficient mice were highly susceptible to intestinal inflammation compared to controls, and IL-22<sup>+</sup>ILC3 levels were significantly reduced in *C. rodentium* infection model. While in the anti-CD40-induced colitis model, although decreased IL-22<sup>+</sup>ILC3 levels were also observed, OLFM4 deficiency significantly ameliorated inflammation, suggesting that the loss of IL-22<sup>+</sup>ILC3 contributes to protection from intestinal inflammation. Considering the importance of IL-22 in intestinal homeostasis and immunity, the functional link between OLFM4 and IL-22 provides a mechanistic understanding of colitis, which may provide a framework for the development of potential therapeutic targets for patients with inflammatory bowel and infectious diseases.

Besides, Th17 cells play an important role in maintaining intestinal homeostasis, resisting bacterial invasion, causing intestinal inflammation. Several studies have shown redundant roles of ILC3s when T cells are present<sup>79</sup>. Lucille C. Rankin showed that NCR<sup>+</sup>ILC3 are redundant for the control of mouse colonic infection in the presence of T cells<sup>80</sup>. However, our research indicates that transferring ILC3s to NCG mice which deficiency in T, B, NK, and ILC cells, can significantly reduce the degree of intestinal damage and mortality caused by *C. rodentium* infection. These results suggest that the role of ILC3 is particularly crucial during the initial phase of infection as it provides protection against damage to the cecum, which serves as the primary site against *C. rodentium* colonization the 5–8 days after infection<sup>81</sup>. In our research, which focuses on acute colitis in 7 days, the impact of OLFM4 on T cells appears to be limited. OLFM4 may also participate in the clearance of *C. rodentium* in the next 20 days and completely eradicated by adaptive immunity. Our previous research has shown that the involvement of OLFM4 extends to both acute and chronic inflammation, as well as the transition from inflammation to cancer in PMN-MDSCs<sup>43</sup>. Next, we may explore the regulatory role of OLFM4 in chronic inflammation in T cells and ILC3.

The gut environment has a significant impact on ILC3s and their responses. For example, microbiota can activate CX3CR1<sup>+</sup> mononuclear phagocytes or CD103<sup>+</sup>CD11b<sup>+</sup> conventional DCs that produce IL-23, IL-1 $\beta$ , and IL-1 $\alpha$ . ILC3s respond to these cytokines and produce IL-22, IL-17, GM-CSF, and IFN- $\gamma$ <sup>15</sup>. Dietary microbiota metabolites such as short-chain fatty acids, oxysterols, and butyrate can directly activate ILC3s through the free fatty acid receptor 2 metabolite receptor<sup>15–17</sup>. Some dietary ligands such as retinoic acid and vitamin D can also regulate ILC3 activity. Compared with that in normal tissues, OLFM4 is abnormally expressed in many pathological tissues. We demonstrated that *C. rodentium* infection significantly increased OLFM4 protein expression in ROR $\gamma$ t<sup>+</sup>ILC3. However, the mechanism by which these microbiotas regulate OLFM4 protein expression in ILC3 remains unclear and requires further investigation.

OLFM4 is widely recognized as a reliable marker for intestinal stem cells<sup>33,41</sup>. In patients with UC, OLFM4 mRNA and protein expression levels are significantly upregulated in the intestinal epithelium<sup>33,39</sup>. OLFM4-deficient mice showed severe inflammation and mucosal damage in the colon following DSS induction<sup>46</sup>, and more severe gastritis was observed after infection with *H. pylori*<sup>82</sup>. Analysis of single-cell sequencing results from patients with UC revealed that OLFM4 is highly expressed in ILC3s. OLFM4 protects intestinal tissues from inflammation caused by barrier damage and pathogen invasion via IL-22-producing ILC3s. However, whether OLFM4 influences ILC3 function in the extracellular environment as a secretory protein remains unclear. Further studies are required to determine whether OLFM4 from IECs regulates ILC3 function in the intestine.



In conclusion, OLFM4 is a novel regulator of IL-22<sup>+</sup>ILC3. OLFM4 contributes to the regulation of ILC3-mediated inflammation. These findings may provide a framework for the discovery of potential therapeutic targets in patients with colitis and other infectious diseases.

## Methods

### Human samples

Peripheral blood samples and colonic mucosa tissues were provided by the Department of Gastroenterology of the Sixth Affiliated Hospital of Sun Yat-sen University (Guangzhou, China). The corresponding research plan and ethical approval were approved by the Clinical Trial Ethics Committee of the Sixth Affiliated Hospital of Sun Yat-sen University (Approval ID: E2022243). Written informed consent was obtained from all the participants or their legal guardians at the time of admission. All ethical regulations relevant to human research participants were followed. Blood samples from healthy controls and patients newly diagnosed with UC. Colonic mucosa was obtained from participants undergoing colonoscopy, and participants excluded from UC and other intestinal diseases were subjected to control group (Control). UC was diagnosed based on the gold standard of endoscopy and biopsy pathological evaluation, and patients who had received any type of treatment in the past 3 months were excluded. Additionally, all participants were screened for hepatitis B virus surface antigen, hepatitis C virus, hog cholera virus, and human immunodeficiency virus antibodies. The Mayo score is used as a quantitative index to evaluate the degree of colitis in patients with UC. The score ranges from 0 to 12, comprising remission (0–2), mild (3–6), moderate (6–10), and severe (11–12).

### Mice

C57BL/6J mice were purchased from the Laboratory Animal Center of Southern Medical University. NCG mice (NOD/ShiLjGpt-Prkdc<sup>em26Cd52</sup>Il2rg<sup>em26Cd22</sup>/Gpt) were purchased from GemPharmatech Co. Ltd. (Nanjing, China). CD45.1 mice (referred to as B6.SJL-*Ptprca*<sup>a</sup>/*Pepcb*/*BoyJ*) were purchased from Casgene Biotech. Co. Ltd (China). Mice genetically deficient in all *Olfm4* (OLF4<sup>-/-</sup>) and OLF4<sup>fl/fl</sup> mice were provided by Professor Zhipeng Zou, Southern Medical University. RORγt-Cre mice were kindly provided by Professor Chen Dong from Tsinghua University. Both male and female mice were used in our study, and sex- and age-matched littermate mice of WT (wild type) or OLF4<sup>fl/fl</sup> were used as controls for OLF4<sup>-/-</sup> and RORC<sup>Cre</sup>OLF4<sup>fl/fl</sup> respectively. For the inhibitor experiment, wild-type (WT) mice were randomly assigned to groups and intraperitoneally injected with SB203580 (5 mg/kg/d), NQDI-1 (1 mg/kg/day) or vehicle control daily for 7 consecutive days. The weight of the mice was monitored daily throughout the experiment. We have complied with all relevant ethical regulations for animal use. All experimental protocols were approved by the Institutional Animal Care and Use Committee of Southern Medical University Experimental Animal Ethics Committee (approval number: L2019179).

### Isolation of mouse colonic LPMCs

After mice were sacrificed and mLNs were removed, the colon was removed and placed in ice-cold PBS. The colon was cut longitudinally, thoroughly washed in ice-cold PBS, and mechanically cut into 1-cm fragments with scissors. The colonic fragments were transferred to HBSS buffer containing 10 mM EDTA (Promega, Madison, WI, USA), 1% penicillin/streptomycin, 1 mM dithiothreitol (Fermentas, Waltham, MA, USA) and cultured at 37 °C for 30 min to remove epithelial cells and mucus. After washing twice with PBS, the colonic tissues were cut into smaller 1 mm pieces and digested in Roswell Park Memorial Institute (RPMI) 1640 containing 5% fetal bovine serum, 1 mg/ml collagenase I (Sigma-Aldrich, St. Louis, MO, USA), 1 mg/ml dispase (Roche, Basel, Switzerland), 100 μg/ml DNase I (Sigma-Aldrich), 1% penicillin/streptomycin and 10 mM HEPES at 37 °C for 45 min. The digested tissues were shaken violently, passed through a 70-μm cell strainer, and resuspended in 40% Percoll (GE Healthcare, Chicago, IL, USA). LPMCs were enriched with 40% / 80% Percoll gradient. After centrifugation at 25 °C, 400 × g for 25 min, the white membrane was aspirated

and washed twice with PBS to obtain the colonic LPMCs for subsequent experiments.

### Flow cytometry

**Cell surface staining.** Single-cell suspensions were stained with a combination of fluorescently conjugated monoclonal antibodies. For surface marker staining, we used antibodies to the following mouse proteins: CD45 (30-F11), CD90.2 (53-2.1), lineage markers (CD3/B220/CD11b/Ly6G/TER-119/CD11c/NK1.1/CD5/CD8a/TCRβ/TCRγδ), CD127, CD4 (GK1.5), CCR6 (29-21.17), NKp46 (29A1.4), NK1.1 (PK136), KLRG1 (2F1). Antibodies against the following human proteins were used: CD45, CD127, lineage markers (CD11b /TCRγδ /TCRαβ /CD14 /CD34 / CD19 /CD3 /CD123 /CD8 /CD5 /CD4 /CD11c /FceR1), CD161, CD117(c-Kit), CRTH2, and NKp44. In human peripheral blood, gating strategy for ILCs: ILC2 gated on CD45<sup>+</sup>Lineage<sup>-</sup>CD127<sup>+</sup>CD161<sup>+</sup>CRTH2<sup>+</sup>, ILC3 gated on CD45<sup>+</sup>Lineage<sup>-</sup>CD127<sup>+</sup>CD161<sup>+</sup>CRTH2<sup>+</sup>CD117<sup>+</sup>, and ILC1 gated on CD45<sup>+</sup>Lineage<sup>-</sup>CD127<sup>+</sup>CD161<sup>+</sup>CRTH2<sup>-</sup>CD117<sup>-</sup>NKp44<sup>-</sup>. In mice, gating strategy for ILCs isolated from the colon LPMC: ILC3 gated on CD45<sup>+</sup>Lineage<sup>-</sup>CD90.2<sup>+</sup>CD127<sup>+</sup>RORγt<sup>+</sup>, ILC1 gated on CD45<sup>+</sup>Lineage<sup>-</sup>CD90.2<sup>+</sup>CD127<sup>+</sup>T-bet<sup>+</sup>. ILC2 gated on CD45<sup>+</sup>Lineage<sup>-</sup>CD90.2<sup>+</sup>CD127<sup>+</sup>GATA-3<sup>+</sup>.

**Intracellular staining.** For transcription factor expression, the isolated cells were stained with surface antigen-antibody, fixed, permeabilized according to the manufacturer's instructions (Tonbo; TNB-0607-KIT), and then intracellularly stained with fluorescently conjugated anti-RORγt, GATA3, and T-bet. To measure the expression of cytokines, the isolated colonic LPMCs were stimulated with 50 ng/ml phorbol-12-myristate 13 acetate (PMA), 1 μg/ml ionomycin, and 1 μg/ml brefeldin A at 37 °C for 5 h. Subsequently, the cells were surface-stained, fixed, permeabilized, and stained with fluorescently conjugated anti-IL-22 and anti-IL-17A antibodies. For the analysis of intracellular signaling in ILC3s, cells were surface-stained, fixed, permeabilized, and stained with fluorescently conjugated anti-p38 MAPK (pT180/ pY182) or anti-p-ASK1 (Ser967) for 30 min at room temperature. An LSR Fortessa flow cytometer (BD Biosciences) was used for stained cell acquisition. Data were analyzed using FlowJo V10.0.7 software. The flow cytometry was performed at the Department of Immunology and Department of Developmental Biology at the School of Basic Medical Sciences, Southern Medical University.

### Cell culture and transfection

The MNK-3 cell line is kindly provided by professor Lian Zhou from Guangzhou University of Chinese Medicine. The cells were cultured in DMEM containing 10% fetal bovine serum and 1% penicillin/streptomycin solution with or without a combination of IL-1β (10 ng/ml), IL-23 (10 ng/ml) and IL-7(10 ng/ml). The successfully constructed plasmid/siRNA was mixed with the auxiliary transfection reagent lipo2000 to transfect cells for 6 h. After 48 h of culture in DMEM, cells were collected for subsequent experiments. All cells were cultured at 37 °C and 5% CO<sub>2</sub>. P38 inhibitor SB203580 and ASK1 inhibitor NQDI-1 were added to a final concentration of 10 μM respectively.

### Cytokine detection

The IL-22 and IL-17 ELISA kits were purchased from Invitrogen (IL-22: 88-7422-22; IL-17:88-7371-22). After stimulation of MNK3 cells with IL-1β, IL-23, and IL-7 for 16 h, the cell supernatant was collected and appropriately diluted. Following the instructions provided in the manual, the ELISA kits were used for detection.

### C. rodentium infection model

Age and sex-matched littermates between 6 and 8 weeks of age were inoculated with 1 × 10<sup>8</sup> CFU of *C. rodentium* suspension by oral gavage after an 8 h fast. The mice were weighed daily and sacrificed on day 7 post-infection. The colon was removed, and its length was measured. To assess

bacterial transmission, spleens and livers of infected mice were collected, weighed, and homogenized. The homogenate was plated at serial dilutions onto MacConkey agar plates, and the number of CFUs was determined after overnight incubation at 37 °C.

### DSS-induced colitis model

Age and sex-matched littermates between 6 and 8 weeks of age were used. DSS (MW 36000–50000 Da; MP Biomedicals, Solon, OH, USA) was dissolved in drinking water 2.5% (w/v) for 5 days, and then regular water was consumed for 2 days. Weight loss, fecal consistency, and hematochezia of the mice were monitored daily. Mice were analyzed on day 8. DAI (Disease Activity Index) standard for evaluation: Weight Loss Percentage: Weight loss of 0–5% is assigned a score of 1, weight loss of 5–10% is assigned a score of 2, weight loss of 10–15% is assigned a score of 3, and weight loss of more than 15% is assigned a score of 4. Consistency of Stool: normal stool is assigned a score of 0, loose stool is assigned a score of 2, and diarrhea is assigned a score of 4. Blood in Stool: Normal stool is assigned a score of 0, occult blood is assigned a score of 2, and obvious blood is assigned a score of 4. Add up the scores for the three indicators mentioned above.

### Anti-CD40 model of colitis

Age and sex-matched littermates between 6 and 8 weeks of age were intraperitoneally injected with monoclonal anti-CD40 antibody (150 µg per mouse, FGK45; Bio X Cell, Lebanon, NH, USA). After 7 days, the mice were sacrificed for analysis.

### Cell isolation

Mononuclear cells were firstly isolated from intestine of mice and colonic mucosa of human samples, then ILC3s were obtained using FACS Aria cell sorter (Human ILC3s were identified by lineage<sup>−</sup>CD127<sup>+</sup>CRTH2<sup>−</sup>c-kit<sup>+</sup>, and mice ILC3s were identified by lineage<sup>−</sup>CD45<sup>low</sup>CD90<sup>high</sup>).

### ILC3 adoptive transfer into NCG mice

Intestinal LPLs were firstly isolated, and stained for lineage markers (CD3/B220/CD11b/Ly6G/TER119/CD11c/NK1.1/CD5/CD8a/TCRβ/TCRγδ), CD45, and CD90.2. After washing with FACS buffer, cells were re-suspended in FACS buffer containing 7-AAD. Lin<sup>−</sup>CD90<sup>high</sup>CD45<sup>low</sup> ILC3s were sorted by using a FACS Aria cell sorter. OLFM4<sup>−/−</sup> and WT mice were infected with *C. rodentium* by oral gavage. Intestinal ILC3s were sorted at day 6 by flow cytometry and transferred by tail vein injection into *C. rodentium* infected NCG mice (5×10<sup>4</sup> cells per mouse each time) at 0 and 2 dpi. Mice were sacrificed at day 7 and intestinal samples were harvested for analysis.

### Bone marrow chimeras

CD45.1 recipient mice were lethally irradiated with two doses of 450 rad from X-ray with a resting period of 4 h. Donor mice (CD45.1) and OLFM4<sup>−/−</sup> or control mice (CD45.2) were sacrificed. The bone marrow was harvested from the murine hind limb and suspended in RPMI-1640 culture medium. The BM cells were passed through a 70 µm cell strainer, followed by centrifugation (500 g, 5 min), and then underwent erythrocyte lysis. Cells were washed twice in PBS and filtered through a 40 µm strainer. The donor cells from CD45.1 mice and OLFM4<sup>−/−</sup> or control mice were mixed in a 1:1 ratio. Irradiation recipient mice were injected with 1×10<sup>7</sup> donor cells/200 µl within 6 h by intravenous injection through the tail. The recipient mice should be administered antibiotics in their drinking water for one week prior to irradiation and for one month following irradiation.

### Single-cell RNA-seq (scRNA-seq) data analysis

Published scRNA-seq datasets were accessed in GEO under the accession number SCP259. Downstream analysis clustering and filtering were used to process the outputs with the R package Seurat (version 4.3.1; 10×Genomics). To define the cell types, we performed principal component analysis on the variable genes, and principal components were used for cell clustering. For further ILC3-clustering, cluster markers

(CD45<sup>+</sup>CD3<sup>−</sup>CD4<sup>−</sup>CD56<sup>−</sup>CD11b<sup>−</sup>CD11c<sup>−</sup>CD127<sup>+</sup>CD161<sup>+</sup>CRTH2<sup>−</sup>CD117<sup>+</sup>) were identified using the FindAllMarkers function, and cell types were manually annotated based on the cluster markers. DEGs between two groups were defined as those with *P* < 0.05, as determined using the Welch *t*-test. Single-cell gene expression data were visualized with Volcano Plot in R.

### Immunofluorescence histology

The colon tissue was fixed with 4% paraformaldehyde. 24 h later, it was dehydrated through a gradient of 50%, 70%, 80%, 90%, 95%, and 100% alcohol and xylene. Following embedding in paraffin, the tissue section was rehydrated with xylene and a decreasing gradient of alcohol, then treated with 0.01 M sodium citrate buffer (pH6.0) at 95–98 °C for 15 min for antigen retrieval. After cooling, the tissue was permeabilized with 0.5% Triton X-100 for 20 mins and blocked with a solution of 5% BSA for 1 h. The tissue was incubated overnight with the primary antibody, followed by incubation with the corresponding secondary antibody for one hour. All steps after the antibody-retrieval process were washed three times for 5 min each using PBS solution. The antibodies used for the immunofluorescence analysis are listed in Table S2. The proportion of positive cells and the fluorescence index were measured using NIS viewer software.

### GST pull-down assay

After plasmid construction and verification of all constructs by DNA sequencing analysis, the purified proteins were incubated with MagneGST™ beads (Promega) at 4 °C for approximately 4 h, and then incubated with the cell lysates at 4 °C overnight. Finally, the beads were eluted with sodium dodecyl sulfate buffer, and the supernatants were collected for immunoblot analysis. The antibodies used are listed in Table S2. The primer sequences used for plasmid construction are listed in Table S3.

### Quantitative Real-time PCR

Total RNA was extracted using TRIzol (Catalog No. 15596; Invitrogen, Carlsbad, CA, USA), and reverse transcription was performed using a StarScript II First-strand cDNA Synthesis Kit (catalog no. A212-05; GenStar, Beijing, China) using a ProFlex PCR System (Thermo Fisher Scientific, Waltham, MA, USA). Real-time qPCR was performed using the RealStar Green Power Mixture kit (Catalog No. A314-10; GenStar) using the QuantStudio 6 Flex system (Thermo Fisher Scientific). The mRNA levels were standardized to the relative expression of β-actin in all groups, and the lowest expression level in the control group was artificially set to 1. All experiments were repeated at least twice. The primer sequences used in this study are listed in Supplementary Information Table S3.

### Western blot analysis

Cells were washed with cold PBS and lysed with RIPA buffer containing phosphatase inhibitors and PMSF (1 mM) on ice. Samples were boiled at 98 °C for 15 min and separated by 10% SDS-PAGE. Protein was transferred to a PVDF membrane (Millipore) using a wet transfer system at 100 V for 80 min. After blocking for 1 h in 5% skim milk, membranes were probed with primary antibody overnight at 4 °C and one hour with secondary antibody conjugated to HRP. Protein was visualized using ChemiDoc™ XRS+ (Bio-Rad, Hercules, CA, USA), and intensity was evaluated using Image Lab™ software (Bio-Rad). The antibodies used in this study are listed in Supplementary Information Table S2.

### Immunoprecipitation combined with mass spectrometry (IP-MS)

Cell lysates were incubated with antibodies overnight, and then incubated with beads of Dynabeads® Protein A: Protein G (Cat# 10002D, Life Technologies, Carlsbad, CA, USA) for 4 h. Next, immunoprecipitate was collected. The sample proteins were separated by gel electrophoresis, then obtain the protein gel strips at different positions on the film, extract the peptides after enzymatic digestion, and then the peptide samples were separated by SCIEX's Eksigent ultra 2D model nanoliter liquid chromatograph. The liquid phase chromatography separated peptides were passed to

an ESI tandem mass spectrometer (TripleTOF 5600(SCIEX, Framingham, MA, USA), and finally uses the protein identification software to identify the proteins in the samples.

### Surface plasmon resonance

To measure the interaction between immobilized proteins and flowing proteins, a PlexArray HT A100 SPR instrument (Plexera, Woodinville, WA, USA) was used to monitor the whole procedure in real-time. Briefly, the OLFM4 recombinant protein was immobilized on a CM5 sensor chip (GE Healthcare) and running buffer composed of 10 mM HEPES pH 7.2, 150 mM NaCl, and 0.05% Tween 20. Serial dilutions of MTDH protein were allowed to flow at concentrations ranging from 2000 to 62.5 nM. The resulting data were fitted to a 1:1 binding model using Biacore Evaluation Software (GE Healthcare).

### Statistics and reproducibility

All experimental data were analyzed using GraphPad Prism (version 8.0; GraphPad Software Inc., San Diego, CA, USA). After comparing the distribution of variables, 2-tailed unpaired Student's *t*-tests or non-parametric Mann–Whitney *U* test was used for statistical comparisons. Differences were considered statistically significant at various *P*-values, depending on the experiment (ns, not significant; \**P* < 0.05; \*\**P* < 0.01; \*\*\**P* < 0.001; \*\*\*\**P* < 0.0005). All experiments were conducted for at least three times, with no fewer than three biological replicates for each trial.

### Reagents and antibodies

Details of the reagents and antibodies used in this study are listed in Supplementary Information Tables S1 and S2, respectively.

### Data availability

The data supporting this study's findings are available from the corresponding author upon reasonable request. The source data for all the figures in the manuscript can be found in the supplementary data file. The original blots images are included in the Supplementary Figs. 25–30.

Received: 21 January 2024; Accepted: 18 July 2024;

Published online: 29 July 2024

### References

- Morita, H., Moro, K. & Koyasu, S. Innate lymphoid cells in allergic and nonallergic inflammation. *J. Allergy Clin. Immunol.* **138**, 1253–1264 (2016).
- Ebihara, T. et al. Runx3 specifies lineage commitment of innate lymphoid cells. *Nat. Immunol.* **16**, 1124–1133 (2015).
- Spits, H. et al. Innate lymphoid cells—a proposal for uniform nomenclature. *Nat. Rev. Immunol.* **13**, 145–149 (2013).
- Artis, D. & Spits, H. The biology of innate lymphoid cells. *Nature* **517**, 293–301 (2015).
- Ferreira, A. C. F. et al. RORα is a critical checkpoint for T cell and ILC2 commitment in the embryonic thymus. *Nat. Immunol.* **22**, 166–178 (2021).
- Tindemans, I., Serafini, N., Di Santo, J. P. & Hendriks, R. W. GATA-3 function in innate and adaptive immunity. *Immunity* **41**, 191–206 (2014).
- Schroeder, J.-H., Howard, J. K. & Lord, G. M. Transcription factor-driven regulation of ILC1 and ILC3. *Trends Immunol.* <https://doi.org/10.1016/j.it.2022.04.009> (2022).
- Atreya, I., Kindermann, M. & Wirtz, S. Innate lymphoid cells in intestinal cancer development. *Semin. Immunol.* **41**, 101267 (2019).
- Aujla, S. J. et al. IL-22 mediates mucosal host defense against Gram-negative bacterial pneumonia. *Nat. Med.* **14**, 275–281 (2008).
- Satoh-Takayama, N. et al. Microbial flora drives interleukin 22 production in intestinal NKp46+ cells that provide innate mucosal immune defense. *Immunity* **29**, 958–970 (2008).
- Klose, C. S. & Artis, D. Innate lymphoid cells as regulators of immunity, inflammation and tissue homeostasis. *Nat. Immunol.* **17**, 765–774 (2016).
- Bauché, D. et al. LAG3 Regulatory T Cells Restrain Interleukin-23-Producing CX3CR1 Gut-Resident Macrophages during Group 3 Innate Lymphoid Cell-Driven Colitis. *Immunity* **49**, <https://doi.org/10.1016/j.immuni.2018.07.007> (2018).
- Wang, B. et al. Macrophage β2-Integrins Regulate IL-22 by ILC3s and Protect from Lethal *Citrobacter rodentium*-Induced Colitis. *Cell Rep.* **26**, 1614–1626.e1615 (2019).
- Longman, R. S. et al. CX<sub>3</sub>CR1<sup>+</sup> mononuclear phagocytes support colitis-associated innate lymphoid cell production of IL-22. *J. Exp. Med.* **211**, 1571–1583 (2014).
- Kim, C. H. Control of lymphocyte functions by gut microbiota-derived short-chain fatty acids. *Cell. Mol. Immunol.* **18**, 1161–1171 (2021).
- Emgård, J. et al. Oxysterol Sensing through the Receptor GPR183 Promotes the Lymphoid-Tissue-Inducing Function of Innate Lymphoid Cells and Colonic Inflammation. *Immunity* **48**, 120–132.e128 (2018).
- Chun, E. et al. Metabolite-Sensing Receptor Ffar2 Regulates Colonic Group 3 Innate Lymphoid Cells and Gut Immunity. *Immunity* **51**, 871–884.e876 (2019).
- Kim, M. H., Taparowsky, E. J. & Kim, C. H. Retinoic Acid Differentially Regulates the Migration of Innate Lymphoid Cell Subsets to the Gut. *Immunity* **43**, 107–119 (2015).
- Konya, V. et al. Vitamin D downregulates the IL-23 receptor pathway in human mucosal group 3 innate lymphoid cells. *J. Allergy Clin. Immunol.* **141**, 279–292 (2018).
- Huang, J. et al. Interleukin-17D regulates group 3 innate lymphoid cell function through its receptor CD93. *Immunity* **54**, 673–686.e674 (2021).
- Talbot, J. et al. Feeding-dependent VIP neuron-ILC3 circuit regulates the intestinal barrier. *Nature* **579**, 575–580 (2020).
- Seillet, C. et al. The neuropeptide VIP confers anticipatory mucosal immunity by regulating ILC3 activity. *Nat. Immunol.* **21**, 168–177 (2020).
- Pascal, M. et al. The neuropeptide VIP potentiates intestinal innate type 2 and type 3 immunity in response to feeding. *Mucosal Immunol.* **15**, 629–641 (2022).
- Zhou, L. et al. Innate lymphoid cells support regulatory T cells in the intestine through interleukin-2. *Nature* **568**, 405–409 (2019).
- Zheng, Y. et al. Interleukin-22 mediates early host defense against attaching and effacing bacterial pathogens. *Nat. Med.* **14**, 282–289 (2008).
- Ahlfors, H. et al. IL-22 fate reporter reveals origin and control of IL-22 production in homeostasis and infection. *J. Immunol.* **193**, 4602–4613 (2014).
- Buonocore, S. et al. Innate lymphoid cells drive interleukin-23-dependent innate intestinal pathology. *Nature* **464**, 1371–1375 (2010).
- Li, J. et al. Activation of DR3 signaling causes loss of ILC3s and exacerbates intestinal inflammation. *Nat. Commun.* **10**, 3371 (2019).
- Gehart, H. & Clevers, H. Tales from the crypt: new insights into intestinal stem cells. *Nat. Rev. Gastroenterol. Hepatol.* **16**, 19–34 (2019).
- Ayyaz, A. et al. Single-cell transcriptomes of the regenerating intestine reveal a revival stem cell. *Nature* **569**, 121–125 (2019).
- Grover, P. K., Hardingham, J. E. & Cummins, A. G. Stem cell marker olfactomedin 4: critical appraisal of its characteristics and role in tumorigenesis. *Cancer Metastasis Rev.* **29**, 761–775 (2010).
- Reynolds, A. et al. Canonical Wnt signals combined with suppressed TGFβ/BMP pathways promote renewal of the native human colonic epithelium. *Gut* **63**, 610–621 (2014).
- Gersemann, M. et al. Olfactomedin-4 is a glycoprotein secreted into mucus in active IBD. *J. Crohn's. Colitis* **6**, 425–434 (2012).



34. Mannick, E. E. et al. Gene expression in gastric biopsies from patients infected with *Helicobacter pylori*. *Scand. J. Gastroenterol.* **39**, 1192–1200 (2004).
35. Wang, X., Chen, S., Wang, J. et al. Olfactomedin-4 deletion exacerbates DSS-induced colitis through a matrix metalloproteinase-9-dependent mechanism. *International journal of biological sciences* **19**, 2150–2166 (2023).
36. Guo, X. et al. Induction of innate lymphoid cell-derived interleukin-22 by the transcription factor STAT3 mediates protection against intestinal infection. *Immunity* **40**, 25–39 (2014).
37. Parks, O. B., Pociask, D. A., Hodzic, Z., Kolls, J. K. & Good, M. Interleukin-22 Signaling in the Regulation of Intestinal Health and Disease. *Front. Cell Dev. Biol.* **3**, 85 (2015).
38. Bernshtein, B. et al. IL-23-producing IL-10R $\alpha$ -deficient gut macrophages elicit an IL-22-driven proinflammatory epithelial cell response. *Sci. Immunol.* **4**, <https://doi.org/10.1126/sciimmunol.aau6571> (2019).
39. Smillie, C. S. et al. Intra- and Inter-cellular Rewiring of the Human Colon during Ulcerative Colitis. *Cell* **178**, <https://doi.org/10.1016/j.cell.2019.06.029> (2019).
40. Mangiola, S. et al. Periprostatic fat tissue transcriptome reveals a signature diagnostic for high-risk prostate cancer. *Endocr.-Relat. cancer* **25**, 569–581 (2018).
41. van der Flier, L. G., Haegebarth, A., Stange, D. E., van de Wetering, M. & Clevers, H. OLFM4 is a robust marker for stem cells in human intestine and marks a subset of colorectal cancer cells. *Gastroenterology* **137**, 15–17 (2009).
42. Shinozaki, S. et al. Upregulation of Reg 1 $\alpha$  and GW112 in the epithelium of inflamed colonic mucosa. *Gut* **48**, 623–629 (2001).
43. Chen, Z. et al. OLFM4 deficiency delays the progression of colitis to colorectal cancer by abrogating PMN-MDSCs recruitment. *Oncogene* **41**, 3131–3150 (2022).
44. Li, Y. et al. Cell autonomous expression of BCL6 is required to maintain lineage identity of mouse CCR6+ ILC3s. *J. Exp. Med.* **220**, <https://doi.org/10.1084/jem.20220440> (2023).
45. Serafini, N. et al. Trained ILC3 responses promote intestinal defense. *Science* **375**, 859–863 (2022).
46. Liu, W. et al. Olfactomedin 4 deletion induces colon adenocarcinoma in Apc(Min+) mice. *Oncogene* **35**, 5237–5247 (2016).
47. Singh, A. K. et al. ROR $\gamma$ t-Raftlin1 complex regulates the pathogenicity of Th17 cells and colonic inflammation. *Nat. Commun.* **14**, 4972 (2023).
48. Robinette, M. L. et al. IL-15 sustains IL-7R-independent ILC2 and ILC3 development. *Nat. Commun.* **8**, 14601 (2017).
49. Sugimoto, K. et al. IL-22 ameliorates intestinal inflammation in a mouse model of ulcerative colitis. *J. Clin. Investig.* **118**, 534–544 (2008).
50. Tsai, P. Y. et al. IL-22 Upregulates Epithelial Claudin-2 to Drive Diarrhea and Enteric Pathogen Clearance. *Cell Host Microbe* **21**, 671–681.e674 (2017).
51. Lee, J. S. et al. Interleukin-23-Independent IL-17 Production Regulates Intestinal Epithelial Permeability. *Immunity* **43**, 727–738 (2015).
52. Song, C. et al. Unique and redundant functions of NKp46+ ILC3s in models of intestinal inflammation. *J. Exp. Med.* **212**, 1869–1882 (2015).
53. Yu, H. B. et al. Vasoactive intestinal peptide promotes host defense against enteric pathogens by modulating the recruitment of group 3 innate lymphoid cells. *Proc Natl Acad Sci USA* **118**, <https://doi.org/10.1073/pnas.2106634118> (2021).
54. Uhlig, H. H. et al. Differential activity of IL-12 and IL-23 in mucosal and systemic innate immune pathology. *Immunity* **25**, 309–318 (2006).
55. Eken, A., Singh, A. K., Treuting, P. M. & Oukka, M. IL-23R+ innate lymphoid cells induce colitis via interleukin-22-dependent mechanism. *Mucosal Immunol.* **7**, 143–154 (2014).
56. Seshadri, S., Allan, D. S. J., Carlyle, J. R. & Zenewicz, L. A. Bacillus anthracis lethal toxin negatively modulates ILC3 function through perturbation of IL-23-mediated MAPK signaling. *PLoS Pathog.* **13**, e1006690 (2017).
57. Matsuzawa, A. et al. ROS-dependent activation of the TRAF6-ASK1-p38 pathway is selectively required for TLR4-mediated innate immunity. *Nat. Immunol.* **6**, 587–592 (2005).
58. Morita, K. et al. Negative feedback regulation of ASK1 by protein phosphatase 5 (PP5) in response to oxidative stress. *EMBO J.* **20**, 6028–6036 (2001).
59. Goldman, E. H., Chen, L. & Fu, H. Activation of apoptosis signal-regulating kinase 1 by reactive oxygen species through dephosphorylation at serine 967 and 14-3-3 dissociation. *J. Biol. Chem.* **279**, 10442–10449 (2004).
60. Kim, A. H., Khursigara, G., Sun, X., Franke, T. F. & Chao, M. V. Akt phosphorylates and negatively regulates apoptosis signal-regulating kinase 1. *Mol. Cell. Biol.* **21**, 893–901 (2001).
61. Hayakawa, Y. et al. Apoptosis signal-regulating kinase 1 regulates colitis and colitis-associated tumorigenesis by the innate immune responses. *Gastroenterology* **138**, <https://doi.org/10.1053/j.gastro.2009.11.015> (2010).
62. Allan, D. S. J. et al. An in vitro model of innate lymphoid cell function and differentiation. *Mucosal Immunol.* **8**, 340–351 (2015).
63. Xiong, L. et al. Group 3 innate lymphoid cell pyroptosis represents a host defence mechanism against Salmonella infection. *Nat. Microbiol.* **7**, 1087–1099 (2022).
64. Peng, V. et al. Ornithine decarboxylase supports ILC3 responses in infectious and autoimmune colitis through positive regulation of IL-22 transcription. *Proc. Natl Acad. Sci. USA* **119**, e2214900119 (2022).
65. Zhu, S. et al. Diet-Induced Hyperhomocysteinaemia Increases Intestinal Inflammation in an Animal Model of Colitis. *J. Crohn's. colitis* **9**, 708–719 (2015).
66. Monteleone, I. et al. Sodium chloride-enriched Diet Enhanced Inflammatory Cytokine Production and Exacerbated Experimental Colitis in Mice. *J. Crohn's. Colitis* **11**, 237–245 (2017).
67. Welin, A. et al. The human neutrophil subsets defined by the presence or absence of OLFM4 both transmigrate into tissue in vivo and give rise to distinct NETs in vitro. *PLoS One* **8**, e69575 (2013).
68. Liu, W., Chen, L., Zhu, J. & Rodgers, G. P. The glycoprotein hGC-1 binds to cadherin and lectins. *Exp. Cell Res.* **312**, 1785–1797 (2006).
69. Rosenbauer, F. et al. pDP4, a novel glycoprotein secreted by mature granulocytes, is regulated by transcription factor PU.1. *Blood* **103**, 4294–4301 (2004).
70. Wang, L. et al. MTDH Promotes Intestinal Inflammation by Positively Regulating TLR Signalling. *J. Crohn's. colitis* **15**, 2103–2117 (2021).
71. Liu, W.-T. et al. Metadherin facilitates podocyte apoptosis in diabetic nephropathy. *Cell Death Dis.* **7**, e2477 (2016).
72. Guia, S. & Narni-Mancinelli, E. Helper-like Innate Lymphoid Cells in Humans and Mice. *Trends Immunol.* **41**, 436–452 (2020).
73. Zeng, B. et al. ILC3 function as a double-edged sword in inflammatory bowel diseases. *Cell Death Dis.* **10**, 315 (2019).
74. Wang, X. et al. GPR34-mediated sensing of lysophosphatidylserine released by apoptotic neutrophils activates type 3 innate lymphoid cells to mediate tissue repair. *Immunity* **54**, <https://doi.org/10.1016/j.immuni.2021.05.007> (2021).
75. Pearson, C. et al. ILC3 GM-CSF production and mobilisation orchestrate acute intestinal inflammation. *eLife* **5**, e10066 (2016).
76. Teunissen, M. B. M. et al. Composition of innate lymphoid cell subsets in the human skin: enrichment of NCR(+) ILC3 in lesional skin and blood of psoriasis patients. *J. investigative Dermatol.* **134**, 2351–2360 (2014).
77. Bernink, J. H. et al. c-Kit-positive ILC2s exhibit an ILC3-like signature that may contribute to IL-17-mediated pathologies. *Nat. Immunol.* **20**, 992–1003 (2019).



78. Bernink, J. H. et al. Interleukin-12 and -23 Control Plasticity of CD127(+) Group 1 and Group 3 Innate Lymphoid Cells in the Intestinal Lamina Propria. *Immunity* **43**, 146–160 (2015).
79. Xiong, L., Nutt, S. L. & Seillet, C. Innate lymphoid cells: More than just immune cells. *Front. Immunol.* **13**, 1033904 (2022).
80. Rankin, L. C. et al. Complementarity and redundancy of IL-22-producing innate lymphoid cells. *Nat. Immunol.* **17**, 179–186 (2016).
81. Stockinger, B. T cell subsets and environmental factors in *Citrobacter rodentium* infection. *Curr. Opin. Microbiol.* **63**, 92–97 (2021).
82. Liu, W. et al. Olfactomedin 4 down-regulates innate immunity against *Helicobacter pylori* infection. *Proc. Natl Acad. Sci. USA* **107**, 11056–11061 (2010).

## Acknowledgements

We thank professor Z.P. Zou, Southern Medical University, for providing OLFM4<sup>fllox/fllox</sup> mice, professor C. Dong from Tsinghua University for providing ROR $\gamma$ t-Cre mice and professor L. Zhou from Guangzhou University of Chinese Medicine for providing the MNK3 ILC3 cell line. This work was supported by grants from the following institutions: the National Natural Science Foundation of China (grant numbers 82171706 and 81991511), National Natural Science Foundation of Guangdong (grant numbers 2022A1515012427, 2022A1515140172, and 2024A1515012897), and Open Fund Project of Guangdong Academy of Medical Sciences (grant number YKY-KF202209). The flow cytometry used in this work was supported by the Department of Immunology at the School of Basic Medical Sciences, Southern Medical University.

## Author contributions

Z. Xing, X.-Y. Li, J.-Y. He and Y.-M. Chen designed and performed most of the experiments and analyzed the data. L. Zhu, X.-G. Zhang, Z.-C. Huang, J. Tang and Y.-X. Guo participated in the experimental design and edited the manuscript. Y.-M. He conceived and supervised the study, interpreted the experiments, and wrote the paper.

## Competing interests

The authors declare no competing interests.

## Additional information

**Supplementary information** The online version contains supplementary material available at <https://doi.org/10.1038/s42003-024-06601-y>.

**Correspondence** and requests for materials should be addressed to Jian Tang, Yuxiong Guo or Yumei He.

**Peer review information** *Communications Biology* thanks the anonymous reviewers for their contribution to the peer review of this work. Primary Handling Editors: Connie Wong and Manuel Breuer. [A peer review file is available.]

**Reprints and permissions information** is available at <http://www.nature.com/reprints>

**Publisher's note** Springer Nature remains neutral with regard to jurisdictional claims in published maps and institutional affiliations.

**Open Access** This article is licensed under a Creative Commons Attribution-NonCommercial-NoDerivatives 4.0 International License, which permits any non-commercial use, sharing, distribution and reproduction in any medium or format, as long as you give appropriate credit to the original author(s) and the source, provide a link to the Creative Commons licence, and indicate if you modified the licensed material. You do not have permission under this licence to share adapted material derived from this article or parts of it. The images or other third party material in this article are included in the article's Creative Commons licence, unless indicated otherwise in a credit line to the material. If material is not included in the article's Creative Commons licence and your intended use is not permitted by statutory regulation or exceeds the permitted use, you will need to obtain permission directly from the copyright holder. To view a copy of this licence, visit <http://creativecommons.org/licenses/by-nc-nd/4.0/>.

© The Author(s) 2024

<sup>1</sup>Pediatric Intensive Care Unit, Guangdong Provincial People's Hospital (Guangdong Academy of Medical Sciences); Department of Immunology, School of Basic Medical Sciences; Department of Clinical Laboratory, the Third Affiliated Hospital of Southern Medical University, Southern Medical University, Guangzhou, China.

<sup>2</sup>Department of Immunology; Guangdong Provincial Key Laboratory of Single Cell Technology and Application, School of Basic Medical Sciences; Southern Medical University, Guangzhou, China. <sup>3</sup>Institute of Thoracic Oncology and Department of Thoracic Surgery, West China Hospital, Sichuan University, Chengdu, China.

<sup>4</sup>Department of Gastroenterology, the Sixth Affiliated Hospital, Sun Yat-sen University, Guangzhou, China. <sup>5</sup>Guangdong Provincial Key Laboratory of Colorectal and Pelvic Floor Diseases, the Sixth Affiliated Hospital, Sun Yat-sen University, Guangzhou, China. <sup>6</sup>Biomedical Innovation Center, The Sixth Affiliated Hospital, Sun Yat-sen University, Guangzhou, China. <sup>7</sup>Pediatric Intensive Care Unit, Guangdong Provincial People's Hospital (Guangdong Academy of Medical Sciences), Southern Medical University; Guangdong Provincial Cardiovascular Institute, Guangdong Provincial People's Hospital, Guangdong Academy of Medical Sciences, Guangzhou, China.

<sup>8</sup>These authors contributed equally: Zhe Xing, Xinyao Li, Junyu He, Yimin Chen. <sup>9</sup>These authors jointly supervised this work: Jian Tang, Yuxiong Guo, Yumei He.

✉ e-mail: [tangj33@mail.sysu.edu.cn](mailto:tangj33@mail.sysu.edu.cn); [guoyuxiong@gdph.org.cn](mailto:guoyuxiong@gdph.org.cn); [hym0909@smu.edu.cn](mailto:hym0909@smu.edu.cn)